REVIEWS OF GEOPHYSICS AND SPACE PHYSICS, VOL. 20, NO. 4, PAGES 827–849, NOVEMBER 1982

Thermodynamics and Lattice Vibrations of Minerals: 5. Applications to Phase Equilibria, Isotopic Fractionation, and High-Pressure Thermodynamic Properties

SUSAN WERNER KIEFFER

U.S. Geological Survey, Flagstaff, Arizona 86001

In previous papers in this series, a model that uses available elastic, structural, and spectroscopic data on minerals has been used to predict the thermodynamic functions C_V (heat capacity), S (entropy), E (internal energy), and F (Helmholtz free energy). In this paper, four applications to problems of current geochemical and geophysical interest are presented: (1) interpretation of complex trends of calorimetric data; (2) calculation of phase equilibria; (3) calculation of oxygen-isotopic fractionation factors; and (4) estimation of the effect of pressure on thermodynamic functions. The model demonstrates that trends in high-temperature thermodynamic properties of silicates are determined by the position and relative numbers of high-frequency modes, generally antisymmetric (Si, Al)-O stretching modes. The position of these modes varies systematically with degree of polymerization of tetrahedra, and therefore high-temperature calorimetric behavior is relatively systematic as a function of crystal structure and mineral composition. Trends at low frequency are much more complex because the low-frequency optic modes that most strongly influence the low-temperature thermodynamic functions depend in a complex way on the size, coordination, and mass of cations and various polyhedra in the minerals. The heat capacity curves of kyanite, andalusite, and sillimanite and of quartz, coesite, and stishovite show crossovers that cannot be explained by Debye theory, which accounts only for acoustic mode behavior, but can be explained by the model spectra proposed because proper account is taken of the changing low- and high-frequency optic modes upon polymorphic transformations. The proposed model is sufficiently accurate that phase equilibrium problems can be addressed: the quartz-coesite-stishovite equilibrium curves, the kyanite-andalusite-sillimanite triple point, and the breakdown of albite to jadeite-plus-quartz are cited as specific examples. For each example, predicted slopes of equilibrium curves agree moderately well to excellently with slopes determined experimentally. The calculated slopes are sensitive to spectroscopic parameters, particularly to the distribution of optic modes in the far infrared; this sensitivity is discussed in detail for the albite breakdown reaction. The model can be used for prediction of isotopic fractionation factors if spectra of the isotopic forms of the mineral are known or postulated. A simple set of 'rules' for generating hypothetical spectra of ^{18}O minerals from measured spectra of the ^{16}O forms is given. Reduced partition functions are calculated for 13 minerals. At 298°K the model values of reduced partition function, 1000 ln α, of these minerals decrease in the order quartz > calcite ≳ albite > muscovite > clinoenstatite ≈ anorthite > diopside > pyrope > grossular > zircon > forsterite > andradite > rutile, in good agreement with experimental data. At 1000°K the first six minerals show small crossovers so that the order becomes calcite, muscovite ≈ albite, quartz, anorthite, and clinoenstatite; the differences in 1000 ln α at high temperature for these minerals are so small that the model probably cannot address the deviations from experimental trends. The model clearly defines the region in which the fractionation factors do not follow a $1/T^2$ trend and should be useful for extrapolation of experimental data to low temperatures. Finally, a modified Grüneisen parameter model is proposed for shift of the lattice vibrational frequencies under compression, and thermodynamic properties to 1000 kbar, 1000°K, are given for nine minerals. At 1 Mbar, the predicted decrease in entropy at 298°K ranges from 54% (of the 1-bar value) for periclase to 25% for stishovite.

CONTENTS

Paper number 2R1228.

1. INTRODUCTION

A model for estimating thermodynamic properties of minerals from elastic, structural, and spectroscopic data was proposed in the first four papers of this series [*Kieffer*, 1979*a*, *b*, *c*, 1980] (hereinafter referred to as papers 1, 2, 3, and 4). The purpose of this paper is to illustrate, in a general way, application of the model to geologic problems of interest.

Four applications of the model are given in this paper: (1) interpretation of complex trends of calorimetric data and prediction of thermodynamic properties of minerals for which calorimetry cannot be performed; (2) calculation of phase equilibria; (3) prediction of oxygen isotopic fractionation factors; and (4) estimation of the effect of pressure on thermodynamic functions.

For detailed applications in problems of current research, knowledge of mineral properties beyond the scope of the particular thermodynamic study of papers 1–4 is often required: for example, phase equilibria calculations may require inclusion of order-disorder phenomena, and magnetic or configurational effects; isotopic fractionation calculations may require consideration of the detailed behavior of compounds containing hydrogen ions or water molecules; and pressure dependence calculations require detailed evaluation of the behavior of the thermal-expansion and Grüneisen parameters, both of which are difficult and controversial subjects. Therefore most of this discussion is meant to be illustrative, using common, well-studied minerals and phase equilibria, in order to demonstrate both the potential and the limitations of the model.

2. Interpretation and Prediction of Thermodynamic Functions

As was mentioned in papers 1–4, the model can be used either to predict heat capacities independently of calorimetric data or to extrapolate heat capacity data to higher and/or lower temperatures than those attained by calorimetric techniques; for example, heat capacities for coesite and stishovite could be predicted above 300°K at which temperature experimental data cannot be obtained because the phases become metastable, and heat capacities can be estimated for many minerals where data below 54°K are not available. For example, *Gaffney* [1982] has used this model to predict the heat capacities of water ices for which calorimetric data are not available. For data extrapolation, a modified model that finds the best fit between any available calorimetric data and a simple vibrational spectrum was suggested for obtaining greater accuracy (paper 4).

The model can also be used to indicate possible inconsistencies among various data sets: for example, calorimetric data on stishovite could not be reproduced using elastic data and reasonable spectroscopic models (paper 3); calorimetric and low-frequency spectroscopic data on enstatite seem to be inconsistent (paper 4); and acoustic velocities estimated for brucite from shock wave data give model heat capacities much higher than measured heat capacities (without including any contribution from optic modes) (paper 3). If the measured brucite heat capacity data are correct, the inference would be that the estimated wave velocities are too

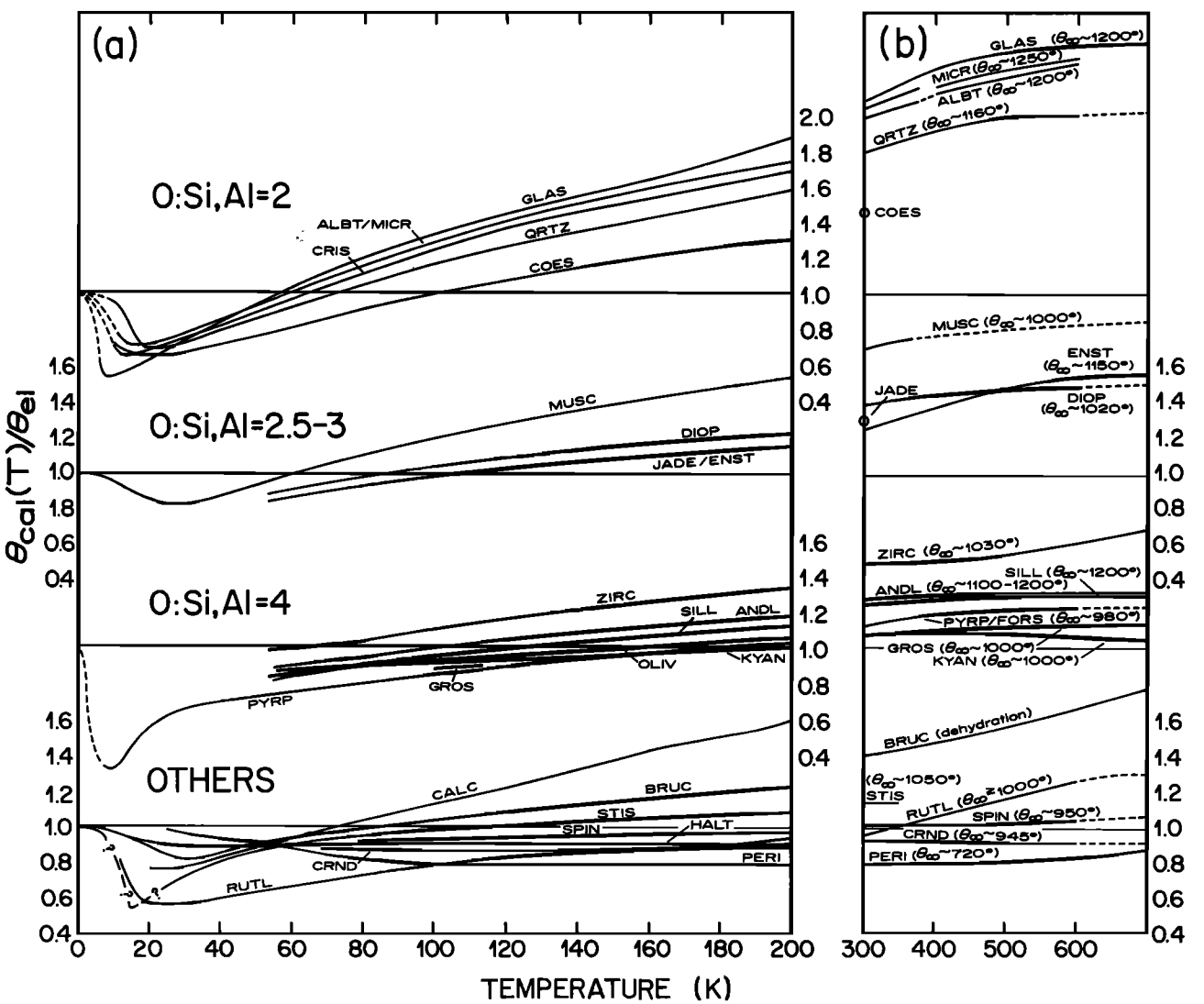

Fig. 1. Curves of $\theta_{cal}(T)/\theta_{el}$ versus T for (*a*) low-temperature heat capacity data and (*b*) high-temperature data (abscissa scale of Figure 1*b* is different from that of Figure 1*a*). See Figure 4, paper 1, for notes and references.

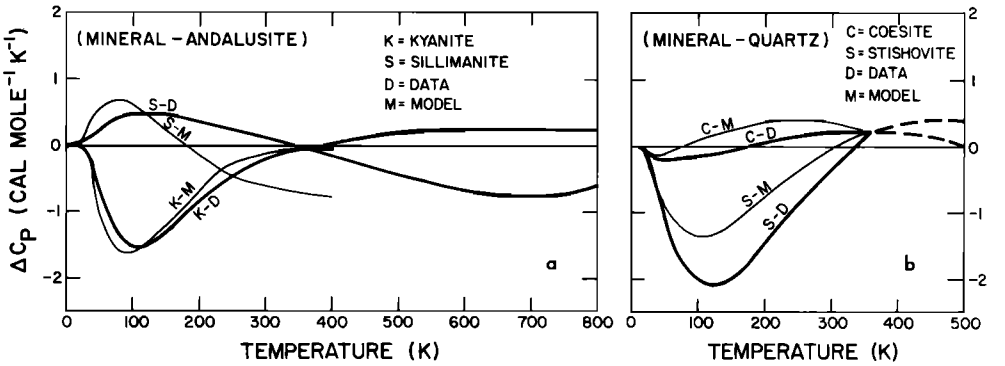

Fig. 2. (*a*) Heat capacity deviations for Al_2SiO_5 polymorphs; kyanite and andalusite data are from R. Robie and B. Hemingway (personal communication, 1981), and sillimanite data are from *Todd* [1950]. Model values are from paper 4. (*b*) Heat capacity deviations for SiO_2 polymorphs. Data for quartz are from *Lord and Morrow* [1957]; data for coesite and stishovite are experimental data of *Holm et al.* [1967] to 350°K. Values beyond this are from model. For stishovite, model 2 of paper 3 was used, and, for coesite, model 1 of paper 3 because these models gave the best match to experimental C_P* data at 300°–350°K.

low. In model calculations for albite and sillimanite, calorimetric data (presumed accurate) could not be matched by model calculations using spectral data (infrared only) available at the time (papers 3 and 4). Additional low-frequency vibrations were required to fit the heat capacity data, and so we obtained Raman spectra for these minerals. These spectra showed low-frequency Raman lines at 83 cm^{-1} for albite and at 115 cm^{-1} for sillimanite (J. Delany, University of California, Los Angeles, unpublished data, 1978), exactly in positions that brought model values into good agreement with measured values of C_V. One should always keep in mind that one possible cause of apparent inconsistencies between data sets indicated by the model can be that the assumed form of the model spectrum does not adequately resemble the real lattice vibrational spectrum of a mineral. However, the general agreement between predicted and measured thermodynamic functions for 30 minerals examined suggests that use of the model provides a reasonable way to attempt to integrate elastic, spectroscopic, and thermodynamic data sets and that substantial inconsistencies call for reexamination of experimental data sets used.

The model provides insight into observed calorimetric trends given in Figure 4 of paper 1, reproduced as Figure 1 of this paper. The simplified vibrational spectra of the model reveal systematic variations in various groups of modes that appreciably influence the low- and high-temperature thermodynamic functions:

1. Trends at high temperatures (Figure 1*b*) are determined by the position and relative numbers of the highest-frequency modes (antisymmetric (Si, Al)-O stretching modes for most silicates and Al-O, O-H stretching or Si-O modes for some other minerals studied). The position of these modes varies systematically with degree of polymerization of tetrahedra, and therefore high-temperature calorimetric behavior is relatively systematic as a function of crystal structure and mineral composition.

2. Trends at low temperatures (Figure 1*a*) are determined primarily by the position of the lowest-frequency optic modes and secondarily by the magnitude and relative proportion of acoustic modes and their relationship to the optic mode frequencies. Because the position of the lowest-frequency optic modes is sensitive to the size and coordination of cations and various polyhedra in the minerals, low-temperature calorimetric trends are not nearly as systematic as high-temperature trends and must be more cautiously interpreted and predicted in terms of individual mineral properties.

The model predicts absolute values of the thermodynamic functions of minerals better than a Debye or Einstein model and can be used to explain variations of the thermodynamic functions with temperature that these one-parameter models cannot explain. An example discussed in paper 4 was the relation between heat capacity (C_V) and entropy (S) of pyrope and grossular. Measured data show that the heat capacity of pyrope at 298°K is less than that of grossular, whereas the entropy is greater. This anomaly occurs because of relations in the low-frequency part of the spectrum and is nearly reproduced by the theoretical model (which predicts that the heat capacities will be about equal instead of reversed from the entropies). Comparison of pyrope and grossular model spectra (paper 4) shows that pyrope has a lower-frequency optic mode than grossular, but also a slightly lower average density of optic modes. These two effects oppose each other in contributing to the low-temperature heat capacity, with the net result of the near equality of C_V for pyrope and grossular at low temperature. However, when C_P/T ($\approx C_V/T$ at low temperature) is integrated to give entropy, the entropy of pyrope is greater than the entropy of grossular because the $1/T$ weighting factor in entropy enhances the effect of the lower-frequency modes of pyrope.

Consider two additional examples of thermodynamic behavior that cannot be explained by a simple Debye model: crossovers in the heat capacities of kyanite, andalusite, and sillimanite and similar crossovers in the heat capacities of quartz, coesite, and stishovite illustrated in Figures 2*a* and 2*b*. In these figures, deviation curves showing measured and calculated heat capacity differences between mineral pairs are shown. Even in the lowest temperature range where the model is least accurate, these curves reproduce well the trends of the deviation curves and, reasonably well, their magnitudes. Therefore interpretation of the cause of this behavior in terms of model parameters appears justified.

Consider first the Al_2SiO_5 polymorphs (Figure 2*a*). At temperatures between 54°K and 350°K, their heat capacities increase in the order kyanite, andalusite, sillimanite. The heat capacity curves cross over each other between 350° and

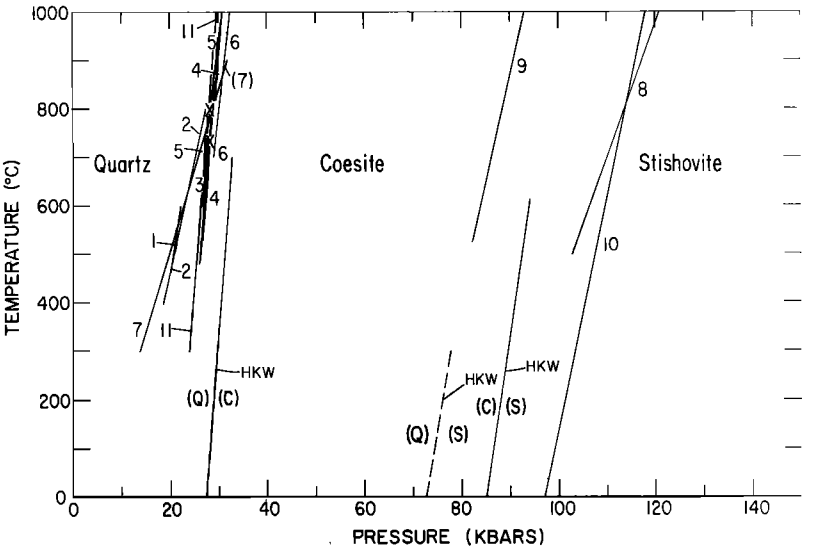

Fig. 3. A partial compilation of data on SiO_2 phase equilibria. Other data can be found in the work by *Weaver et al.* [1979]. The curves are from the following references: (curve 1) *Dachille and Roy* [1959], (curve 2) *MacDonald* [1956], (curve 3) *Takahashi* [1963], (curve 4) *Kitahara and Kennedy* [1964], (curve 5) *Boyd and England* [1960] extrapolated to lower temperatures, (curve 6) *Boyd et al.* [1966] extrapolation of revised curve, (curve 7) *Griggs and Kennedy* [1956], (curve 8) *Ostrovsky* [1967], (curve 9) *Akimoto and Syono* [1969], (curve 10) *Stishov* [1964]; and (curve 11) *Bohlen and Boettcher* [1982]. The two crosses on the quartz-coesite curve are the data of *Boettcher and Wyllie* [1968]. HKW refers to the curves calculated by *Holm et al.* [1967]. *Yagi and Akimoto* [1976] have additional data on coesite-stishovite; from their data one may infer a slope of about 11 bars deg^{-1} from the coesite-stishovite equilibrium [*Weaver et al.*, 1979]. *Jeanloz and Thompson* [1982] prefer a slope of 21 bars deg^{-1}

400°K, and at high temperatures the heat capacities increase in the order sillimanite, andalusite, kyanite. Elastic Debye temperatures of the polymorphs increase in the order andalusite (761°K), sillimanite (782°K), kyanite (916°K). Therefore, according to a Debye model, at all temperatures the relative order of heat capacities should increase from kyanite to sillimanite to andalusite; it does not. The model calculations show that the influence of low-frequency optic modes is sufficiently great at 20°K to upset the relationships expected from acoustic velocities alone. Because the frequency of the lowest optic modes increases in the order sillimanite (115 cm^{-1} at **K** = **0**), andalusite (156 cm^{-1}), and kyanite (237 cm^{-1}) and because the position of these modes dominates heat capacity relationships at low temperatures, the observed order of increasing heat capacity is from kyanite to andalusite to sillimanite. However, the optic modes of kyanite are compressed into a smaller frequency range than those of andalusite and sillimanite (upper cutoff 720 cm^{-1} for kyanite, 780 cm^{-1} for andalusite, and 955 cm^{-1} for sillimanite), so that relationships in heat capacity are reversed as the influence of higher-frequency optic modes becomes important at about room temperature.

The heat capacities of quartz, coesite, and stishovite also show crossovers, as illustrated by the deviation curves of Figure 2*b*. Crossovers in quartz-coesite and quartz-stishovite are indicated by the *Holm et al.* [1967] data; crossovers between coesite and stishovite can be inferred from the trends at the 350°K limit of their data and from my model values. The heat capacity of coesite is much more similar to that of quartz than is the heat capacity of stishovite, because the coordination, and hence the vibrational spectrum, is more similar. The heat capacity of coesite is less than that of quartz at low temperatures because the Debye temperature is higher; however, the frequencies of the optic continuum are lower than for quartz, and thus at relatively low temperatures the heat capacity of coesite rises above that of quartz. At low temperatures, stishovite has a lower heat capacity than either quartz or coesite because it has a very high elastic Debye temperature (hence high acoustic mode frequencies) due to its high density, and also because its lowest optic modes are at relatively high frequencies. However, the heat capacity of stishovite rises more rapidly as temperature rises than that of quartz or coesite because the Si-O stretching modes of stishovite are at lower frequencies (Si in sixfold coordination) than the stretching modes of quartz and coesite (Si in fourfold coordination). Thus at about 300°K, where these stretching modes become effective, the heat capacity of stishovite rises above that of either quartz or coesite.

In general, crossovers in heat capacities and reversals in relative entropy values should be expected for mineral pairs if relative magnitudes of elastic Debye temperatures, and/or frequencies of lowest optic modes or of highest optic modes, show opposing trends. Such opposing trends will be common, for example, across polymorphic phase changes when the influence of the density change is to drive acoustic frequencies upward and the influence of the coordination change is to drive optic frequencies in the opposing direction, downward. *Navrotsky* [1980] recognized that this behavior could occur across polymorphic phase changes in oxides and could give rise to negative pressure-temperature slopes for phase changes in the upper mantle.

3. PHASE EQUILIBRIA

Calculation of phase equilibria provides a more stringent test of the model than calculation of thermodynamic functions alone, because small differences in the thermodynamic functions, rather than their absolute magnitude, determine

TABLE 1. Entropies and Volumes of SiO_2 Phases

Property	α Quartz	β Quartz	Coesite	Stishovite
Volume, $cm^3\ mol^{-1}$				
at 1 bar	22.69	23.72	20.64	14.02
at 30 kbar	21.33	22.29	20.02	13.88
at 70 kbar	19.97	20.87	19.40	13.74
at 90 kbar	19.51	20.40	19.20	13.73
Entropy, cal mol^{-1} $°K^{-1}$ (from model)				
at 298°K	10.08	...	model 1 10.05	7.77[a]
			model 2 9.00	7.65[a]
at 600°K	19.29	...	model 1 19.29	17.19[a]
			model 2 17.86	16.89[a]
at 1000°K	...	27.82	model 1 27.51	25.30[a]
			model 2 25.98	25.14[a]
Entropy, cal mol^{-1} $°K^{-1}$ [from *Robie et al.*, 1978]				
at 298°K	9.91	...	9.65	6.64
at 600°K	19.08	...	18.68	15.74
at 1000°K	...	27.61	26.88	23.88

[a]Anharmonic entropy correction uncertain.

the phase relations. Therefore errors resulting from averaging assumptions in the model become quantitatively important. The following equilibria are examined: quartz-coesite-stishovite, kyanite-andalusite-sillimanite, and albite-jadeite-quartz.

SiO_2 Polymorphs (Quartz, Coesite, Stishovite)

Experiments have suggested a wide range of stability fields for quartz, coesite, and stishovite (Figure 3). Isobaric temperature uncertainties are of the order of 500°K for the univariant equilibrium curves. The quartz-coesite equilibrium is difficult to determine experimentally because of the notorious sluggishness of the quartz-coesite reaction. The coesite-stishovite equilibrium is difficult to determine because the high pressures at which it occurs are difficult to obtain and to calibrate. The metastable quartz-stishovite transition, of considerable interest to shock wave geophysicists and astrogeologists (see *Kieffer et al.* [1976], for example), has only been determined by calculation from calorimetric data. The data of Figure 3 show, however, that slopes of the equilibrium curves are less certain than their position in *P-T* space. The slopes of the equilibrium curves are related to entropy and volume through the Clapeyron relation:

$$dP/dT = \Delta S/\Delta V \quad (1)$$

Because my model predicts only entropies of the phases, not free energies of transition, I will focus only on calculated slopes of equilibrium curves in this section to compare with the slopes determined experimentally.

I have calculated the slopes for the quartz-coesite-stishovite equilibria from entropies calculated at 1000°K, 1 bar, and from volumes appropriate to the approximate pressures of the transitions: 30 kbar for quartz-coesite, 70 kbar for metastable quartz-stishovite, and 90 kbar for coesite-stishovite. (Although a method of obtaining the thermodynamic functions at high pressure is given in section 5, not enough data exist on the thermal expansions of coesite and stishovite to allow it to be used for this calculation.) The entropies and volumes used are listed in Table 1. A model entropy for β quartz was obtained by taking the model value for α quartz at 1000°K (22.69 cal mol^{-1} $°K^{-1}$) and adding 0.13 cal mol^{-1} $°K^{-1}$ for an approximate entropy of transition.

Consider, first, the quartz-coesite equilibrium. Experimentally determined curves show a wide range in slopes (2 to 37 bars deg^{-1} have been proposed); some of the measured equilibrium curves are shown in Figure 3. However, *Boettcher and Wyllie* [1968] and *Weaver et al.* [1979] have critically discussed experimental data, pointing out that the curves having the highest slopes (curves 1, 2, and 7) are generally considered unreliable. *Weaver et al.* [1979] preferred a slope of 13 bars deg^{-1}; *Bohlen and Boettcher* [1982] prefer ~ 8 bars deg^{-1}. The two models proposed for the vibrational spectrum of coesite in paper 3 give substantially different values of entropy and, consequently, quite different values of slope of the phase boundary. The entropy difference between quartz and coesite is so small that the large uncertainties in the thermal expansion, reflected in anharmonic entropy, appreciably affect the calculated slope. The slopes obtained from models 1 and 2 are 6 and 34 bars deg^{-1}, respectively. The latter value is probably not to be considered seriously because the model values of heat capacity are so far from measured values on coesite (on the other hand, *Weaver et al.* [1979] showed that some problems may also exist with the coesite calorimetry). Although the model value of 6 bars deg^{-1} is slightly lower than that preferred by experimentalists for this boundary, it is in remarkable agreement given uncertainty in thermal expansions.

Consider, next, the coesite-stishovite equilibrium. Two different vibrational models were examined for stishovite in paper 3. However, these models differed only in their treatment of the higher-frequency optic modes which do not have a strong influence on the entropy. Therefore little difference in entropy at temperatures above 298°K is predicted by the models, and, for simplicity, only model 2 is discussed here. The calculated slope for this transition is 17 bars deg^{-1}. Experimental values range from 11 to 36 bars: *Weaver et al.* [1979] prefer a value between 11 and 23 bars; *Jeanloz and Thompson* [1982] prefer a value of 21 bars deg^{-1}. Given the wide scatter in the experimental curves and

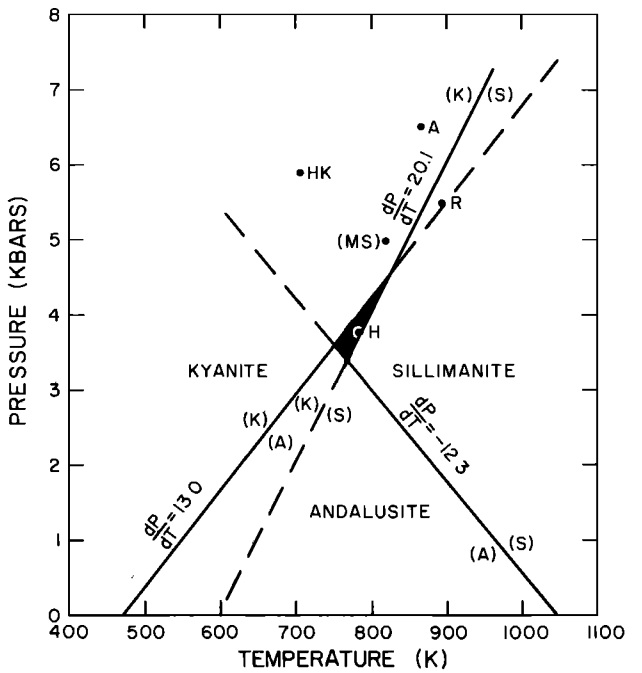

Fig. 4. Calculated slopes of aluminosilicate phase boundaries from model entropies. The intercepts at $P = 0$ were determined from the work of *Holdaway* [1971], as described in the text. The shaded triangular area is bounded by the three phase boundaries; because the slopes of the curves are determined independently from the spectroscopic data, they do not necessarily intercept at a point. Triple points as determined by other investigators are shown: H, *Holdaway* [1971]; HK, *Holm and Kleppa* [1966]; R, *Richardson et al.* [1969]; A, *Althaus* [1967]; (MS), *Mueller and Saxena* [1977], a 'reasonable estimate' from survey of literature.

the small number of data on which they are based, the model value of 17 bars deg^{-1} is probably to be considered satisfactory.

The calculated slope of the metastable quartz-stishovite equilibrium is 15 bars deg^{-1}, less than the slope of 22 bars deg^{-1} that can be inferred from the calorimeter data of *Holm et al.* [1967], as extrapolated by *Robie et al.* [1978]. This difference occurs because my model entropies for stishovite are appreciably greater than those obtained from calorimetry. It is worth noting here that in a recent analysis of existing phase equilibria data on quartz, coesite, and stishovite, *Weaver et al.* [1979] suggested that the entropy of stishovite is 7.7 cal mol^{-1} $°K^{-1}$, in excellent agreement with the values of 7.65 to 7.80 cal mol^{-1} $°K^{-1}$ given by these models in paper 4. This value is about 1 cal mol^{-1} $°K^{-1}$ greater than the calorimetric values, and would give a quartz-stishovite slope close to that predicted above.

Al_2SiO_5 Equilibria

The aluminosilicate phase relations, the subject of much controversy (for example, see *Zen* [1972] and *Day and Kumin* [1980]), provide a very sensitive test of the model because free-energy differences between the phases are very small. Such small differences in free energies (inferred from shapes of stability fields) are somewhat surprising in view of the rather large apparent differences between the vibrational spectrum of sillimanite and the spectra of kyanite and andalusite (paper 2). The Si-O stretching bands of sillimanite cover a much broader range of frequencies than those of the other two polymorphs, extending out to 1200 cm^{-1}, nearly the highest frequencies found for the asymmetric Si-O stretching modes in any silicate. At lower frequencies, spectra of the polymorphs show systematic, although not easily interpretable, differences. The lowest kyanite band is at 237 cm^{-1}, the lowest andalusite band is at 165 cm^{-1}, and the lowest sillimanite band is at 115 cm^{-1}. In effect, spectra are stretched to both lower and higher frequencies as the aluminum coordination progresses from sixfold in kyanite to fourfold in sillimanite. The thermodynamic functions of the polymorphs remain similar in spite of the spectral changes because the stretching in frequency at one end of the spectrum is counteracted by the stretching at the other end.

Calculated entropies for these polymorphs at 298°K are as follows: kyanite, 20.80; andalusite, 23.12; and sillimanite, 23.60 cal mol^{-1} $°K^{-1}$. Molar volumes of the three polymorphs are (in the same order) 44.09, 51.53, and 49.90 cm^3. Therefore the following slopes at 298°K are predicted: sillimanite-andalusite, $dP/dT = -12.3$ bars $°K^{-1}$; andalusite-kyanite; $dP/dT = 13.0$ bars $°K^{-1}$; and sillimanite-kyanite, $dP/dT = 20.1$ bars $°K^{-1}$. For comparison, the slopes preferred by *Holdaway* [1971] at the same temperature are sillimanite-andalusite, −14.0; andalusite-kyanite, 14.2; and sillimanite-kyanite, 19.5 bars $°K^{-1}$.

In order to compare a triple point calculated from model data with triple points of other authors, it is necessary to know the free enthalpies of reaction or, alternately, intercepts of the equilibrium curves at some pressure and temperature. I have adopted intercepts of the phase boundaries at $P = 0$ from *Holdaway* [1971] (Figure 4). Adoption of the $P = 0$ intercepts avoids explicit consideration of Al-Si order-disorder and of curvature of phase boundaries. ΔS is assumed constant over the range of pressure and temperature considered. The heat of reaction $(\Delta H)°_{T_i}$ at the intercept temperature T_i is then implicitly given by

$$T_i(\Delta S)°_{T_i} = (\Delta H)°_{T_i} \tag{2}$$

and a linear equation for a phase boundary becomes

$$P = \frac{[T\Delta S - \Delta H°]}{\Delta V} = \frac{[T - T_i]\Delta S}{\Delta V} \tag{3}$$

Holdaway's intercepts are 1043°K for the andalusite-sillimanite (A-S) boundary, 473°K for the kyanite-andalusite (K-A) boundary, and 599°K for the sillimanite-kyanite boundary. These intercepts, combined with model entropies, give rise to the following phase boundary equations:

K-A

$$P \text{ (bars)} = 13.0[T(°K) - 473]$$

A-S

$$P \text{ (bars)} = -12.3[T(°K) - 1043]$$

S-K

$$P \text{ (bars)} = 20.1[T(°K) - 599]$$

When solved simultaneously, the equilibrium curves intersect each other as follows: A-S and A-K at 750°K = 477°C (P = 3.6 kbars), S-K and A-K at 830°K = 557°C (P = 4.6 kbars), and S-K and A-S at 769°K = 496°C (P = 3.4 kbars).

As shown in Figure 4, a triangular region surrounding the Holdaway triple point is defined by the three model curves. Because the slopes of all three curves obtained from my model are independent, such good convergence toward a

single point is actually quite remarkable. Note that the elongation of the 'triple point' is actually caused by near-parallelism of the kyanite-andalusite and kyanite-sillimanite curves. Thus this example shows that calculation of phase boundary slopes using only spectroscopic and acoustic data and calculation of the phase boundary position using some measure of heats of reaction gives mineral stability fields that are in good agreement with those obtained by other methods, even for polymorphs such as those of Al_2SiO_5 with relatively small free-energy differences.

Stability of Albite

Finally, consider use of the model for computing conditions for the reaction

$$NaAlSi_3O_8 = NaAlSi_2O_6 + SiO_2$$

Experimental determinations of this phase boundary [*Birch and LeComte*, 1960; *Newton and Smith*, 1967; *Hlabse and Kleppa*, 1968; *Boettcher and Wyllie*, 1969; *Johannes et al.*, 1971; *Essene et al.*, 1972; *Hays and Bell*, 1973; *Holland*, 1980] suggest isobaric differences in equilibrium temperature of the order of 300°K at the higher pressures, or isothermal differences of the order of 7 kbar (Figure 5). Curves calculated from calorimetry have an uncertainty of about 1 kbar, largely due to an uncertainty of about 0.5 cal mol^{-1} $°K^{-1}$ in albite and jadeite entropies [*Openshaw*, 1974]. The phase equilibria are complicated by both the degree of ordering in albite (the low-high transition from ordered to disordered probably occurs at $\leq \sim 1000°K$) and the low-high quartz transition (848°K). For this calculation, entropies of low albite and low quartz are used.

The sensitivity of the equilibrium curve to small entropy variations can be seen by consideration of Figure 5. The solid curves represent three different equilibrium lines, each based on the same value of $\Delta H°$ for the reaction, but different values of entropy for the phases. An equilibrium line calculated with calorimetric data obtained for albite by *Kelley et al.* [1953] and calorimetric data for quartz and jadeite by *Robie and Waldbaum* [1968] is given as curve 1. An equilibrium line with the more recent data on albite by *Openshaw* [1974] and the same data for quartz and jadeite is given as curve 2; and an equilibrium line calculated with the *Openshaw* [1974] albite data and my model jadeite entropy values is shown as curve 3. The difference between curves 2 and 3 is caused by the fact that my model jadeite entropy at 298°K is 0.6 cal mol^{-1} $°K^{-1}$ lower than the calorimetric value listed in the work by *Robie and Waldbaum* [1968].

This equilibrium calculation can be used to illustrate how uncertainties in vibrational spectra affect the thermodynamic applications of the model to phase equilibria. The danger of not having adequate or accurate spectra is revealed by such an attempt. The two dashed curves, 4 and 5, in Figure 5 are equilibrium lines computed using model values of entropy for all three minerals. The top one (5) is calculated with the lowest optical mode of albite at 45 cm^{-1}, as suggested in a far-infrared spectrum published by *Kovach et al.* [1975, p. 249]. The bottom dashed curve (4) is one with the lowest optical mode taken at 92 cm^{-1}, as reported by *Iiishi et al.* [1971] (this line is the strongest low-frequency line in the infrared spectrum of albite shown in Figure 1*d* of paper 2). Model values of entropy at 298°K vary by 6 cal mol^{-1} $°K^{-1}$ when these two values of lowest optical mode are used as lower limits of the optic continuum, and the slope of the

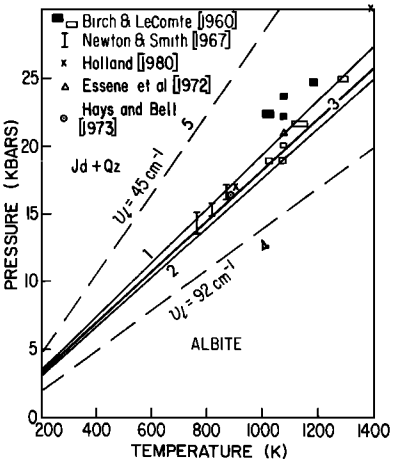

Fig. 5. Measured and calculated phase boundaries for the breakdown of albite to jadeite + quartz. Curves numbered 1–5 are discussed in text.

equilibrium line changes by a factor of 2, accordingly. The lack of agreement between curve 4 and the experimental data suggested that the 92 cm^{-1} line observed by *Iiishi et al.* [1971] was not the lowest-frequency mode. On the other hand, curve 5, based on a line at 45 cm^{-1}, appears to lie considerably higher than most of the reported data. I suspected that there might actually be an optical mode in the vicinity of 80 cm^{-1} that would produce an albite model entropy such that the calculated phase boundary would agree with those boundaries determined from the calorimetric data of either *Kelley et al.* [1953] or *Openshaw* [1974] (curves 1 and 2). The infrared spectrum of albite (paper 2, Figure 1*d*) has a slight band on the low-frequency shoulder of the 92 cm^{-1} band. On the basis of the above hypothesis and this suggestion of the weak band in the infrared spectrum, we obtained a Raman spectrum on albite and found that there is, in fact, a pronounced Raman mode at 83 cm^{-1} (J. Delany, unpublished data, 1978). With this mode taken as the lowest optical frequency at $\mathbf{K} = \mathbf{0}$ and reduced to 63 cm^{-1} at $\mathbf{K} = \mathbf{K}_{max}$, the model entropy at 298°K is within 0.26 cal mol^{-1} $°K^{-1}$ of the value of *Openshaw* [1974], and the calculated equilibrium line is then nearly coincident with curve 1. The experimental data shown, except those of *Birch and LeComte* [1960], are consistent with a lowest optical mode frequency at $\mathbf{K} = \mathbf{0}$ between about 85 and 65 cm^{-1}. Although the spread of values of equilibrium implied by the experimental data in Figure 5 could be due to a number of factors not considered here (variations in jadeite properties, experimental conditions), it is possible that they are due to actual variations in the albite structure that influence the vibrational spectrum and, therefore, the thermodynamic functions. For example, order-disorder effects, if reflected in variations in low-frequency spectral characteristics, could account for the scatter in experimental values.

4. Isotopic Fractionation

Many interesting problems in isotopic thermometry await a theoretical model that can predict the energies of isotopic forms of minerals with sufficient accuracy to allow accurate calculation of isotopic fractionation factors. The energy changes in isotopic exchange reactions are of the order of a few calories per mole and are thus too small to be measured

calorimetrically [*Clayton*, 1981]. Direct measurement by exchange reactions is difficult, particularly at low temperatures, because the driving force for isotopic exchange reactions is small. Therefore experiments must frequently be performed at high temperatures, and the data obtained must be extrapolated to lower temperatures. In the range of temperatures of geologic interest, extrapolation laws are not well understood. Thus even if a theoretical model cannot predict fractionation factors to high accuracy, it might be useful in providing a basis for extrapolation of existing data. In this section I explore the application and limitations of this model to prediction of oxygen isotopic fractionation factors.

Consider [after *Urey*, 1947] an isotopic exchange reaction

$$aA + bB^* = aA^* + bB \tag{4}$$

where a and b are stoichiometric coefficients relative to the exchange reaction, A and B are molecules containing a common element being exchanged, and the asterisk indicates the molecule containing the heavy isotope. For example, in the following reaction between enstatite (px) and olivine (ol),

$$\underset{\text{(px)}}{\tfrac{1}{3}\,MgSi^{16}O_3} + \underset{\text{(ol)}}{\tfrac{1}{4}\,Mg_2Si^{18}O_4} \leftrightarrows \underset{\text{(px)}}{\tfrac{1}{3}\,MgSi^{18}O_3} + \underset{\text{(ol)}}{\tfrac{1}{4}\,Mg_2Si^{16}O_4}$$

the equilibrium constant is [*Clayton*, 1981]

$$K = \frac{(^{18}O/^{16}O)_A}{(^{18}O/^{16}O)_B} = \frac{(^{18}O/^{16}O)_{px}}{(^{18}O/^{16}O)_{ol}}$$

As was shown by *Urey* [1947], the equilibrium constant is related to the free-energy change in the isotopic exchange reaction. From statistical mechanics, the equilibrium constant K for complete exchange of the isotopes is

$$K = (Q_A^*/Q_A)^a \div (Q_B^*/Q_B)^b \tag{5}$$

Q is the partition function for the molecule and is given by

$$Q = \sum_i e^{-E_i/kT} \tag{6}$$

where E_i is the energy of the ith state relative to a rest state with no zero-point energy, k is the Boltzmann constant, and T is the absolute temperature. The summation is taken over all energy levels of the molecule, i.

For a crystalline solid, in the harmonic approximation,

$$E_i = (n + \tfrac{1}{2})h\nu_i \qquad n = 0, 1, 2, \cdots \tag{7}$$

where h is Planck's constant and ν_i is mode frequency. Therefore

$$Q = \prod_{i=1}^{3N-6} \frac{e^{-x_i/2}}{(1 - e^{-x_i})} \tag{8}$$

where $x_i = h\nu_i/kT$, as in paper 3, and N is the number of atoms in the solid.

In exchange reactions, it is ratios of the partition functions that are of interest:

$$\frac{Q^*}{Q} = \prod_{i=1}^{3N-6\approx 3N} \frac{e^{-x_i^*/2}}{(1 - e^{-x_i^*})} \frac{(1 - e^{-x_i})}{e^{-x_i/2}} \tag{9}$$

In the lattice dynamics approximation for crystalline solids, each primitive unit cell vibrates with the same normal modes (see paper 3). Thus a 'reduced' partition function ratio f can be defined for the unit cell; it is equivalent to the partition function originally defined for an ideal gas molecule by *Urey* [1947]:

$$f = \frac{Q^{*\prime}}{Q'} = \frac{Q^*}{Q}\left(\frac{m}{m^*}\right)^{3r/2} \tag{10}$$

where $Q^{*\prime}$ and Q' refer to the partition functions for a unit cell, Q^* and Q refer to the partition functions for a crystalline solid, m and m^* are the masses of exchanging isotopes, r is the number of atoms being exchanged in the unit cell, and the product over $3N$ in equation (9) for Q^*/Q becomes a product over $3s$, the number of degrees of freedom in the primitive cell [*Becker*, 1971]. The reduced partition function ratio corresponds to an equilibrium constant for the exchange reaction between the unit cell and its separated atoms. For convenience, the reduced partition function ratio is usually written in terms of natural logarithms as $(1/r)1000 \ln f$. *Bigeleisen and Mayer* [1947] showed that $\ln f \propto (1/T)^2$ as $T \to \infty$; that is, there is no fractionation at high temperatures. At low temperatures, $\ln f \propto 1/T$ [e.g., *Hulston*, 1978, p. 212].

The Helmholtz free energy of a material is related to the partition function by

$$F = kT \ln Q \tag{11}$$

If the molecules A and B contain isotopes X and X^*, the fractionation factor α of the isotopes is

$$\alpha = \frac{([X^*/X])_{AX_n - AX_n^*}}{([X^*/X])_{BX_m - BX_m^*}} \tag{12}$$

where $[X^*/X]$ denotes the ratio of the isotopes in the compounds subscripted. If the X isotopes are randomly distributed in the unit cells, *Epstein* [1959] has shown that

$$\alpha = K^{1/r} \tag{13}$$

where r is the number of atoms of the element undergoing exchange in (4). From (11),

$$\ln \frac{Q^*}{Q} = \frac{F^* - F}{-kT} \tag{14}$$

Thus the partition function ratio or fractionation factor can be calculated directly from values of F and F^*:

$$\ln f = \frac{F^* - F}{-kT} + \frac{3r}{2} \ln \frac{m}{m^*} \tag{15}$$

From papers 1 and 3,

$$F = 3\eta N_A\beta + kT\int_0^{\omega_l} \ln\{1 - [\exp(-\hbar\omega/kT)]\} g(\omega)\, d\omega \tag{16}$$

where

$$3nN_A\beta = -V_0 - \tfrac{1}{2}\sum_{r=1}^{3N_An} \hbar\omega \tag{17}$$

In these equations I have switched from ν to ω to preserve the identities from paper 3. V_0 is the potential energy of the equilibrium configuration of the crystal, the summation term is the zero-point energy term, ω is the angular frequency, N_A is Avogadro's number, $\hbar = h/2\pi$, n is the number of atoms in

the chemical formula of the compound, $g(\omega)$ is the frequency distribution of normal modes, and ω_l is the highest lattice vibrational frequency. A similar equation holds for F^* with the spectrum $g(\omega)$ being replaced by $g^*(\omega)$ for the isotopically heavy compound.

The equations above, and the methods described below, could be applied to fractionation of many different isotopes such as those of oxygen, sulfur, and silicon. Further discussion, however, is restricted to oxygen-isotope substitution.

The problem facing the theoretician is to specify the frequency distributions $g(\omega)$ and $g^*(\omega)$ for isotopically light and heavy minerals. The most common approach to this problem has been one in which detailed lattice dynamics models are formulated, and force constants for the isotopically light compounds are evaluated from spectroscopic and elastic-wave velocity data. The models are used to predict vibrational frequencies of isotopically heavy species (for example, see *Bottinga* [1968, 1969], *Lambert* [1975], *Becker* [1971], *Kawabe* [1978], *Elcombe* [1974], *Elcombe and Hulston* [1975], and *Hulston* [1978]). Such methods allow detailed treatment of individual minerals but have been limited in application because of their complexity. *Taylor and Epstein* [1962] showed that complex silicates show trends in fractionation that can be explained from knowledge of the types of oxygen bonds, and they were able to estimate $\delta^{18}O$ values by linear combination of bond types. *Sakai and Honma* [1969] were able to calculate mineral-water fractionation factors for 10 minerals simply from examination of the Si-O modes without detailed knowledge of the spectra.

In the approach that follows, I have adopted a model intermediate between detailed spectroscopic calculations and less detailed Si-O bond models. I assume that lattice vibrational spectra $g(\omega)$ of isotopically light minerals can be approximated from spectroscopic and elastic data as described in papers 1–4. A hypothetical spectrum $g^*(\omega)$ is then generated for the isotopically heavy mineral from a set of rules (given below) describing expected frequency shifts for different types of vibrational modes upon substitution of a heavy isotope into the mineral structure. The required integrations and normalizations to (15) and (16) can then be performed to give the reduced partition function ratio (1000 ln f) or, with an assumed partition function for water, a mineral-water fractionation factor, (1000 ln α). The method assumes that vibrational modes are describable in terms of fairly simple atomic motions. While this has been a common practice in spectroscopy, it is certainly not a universally accepted practice, and as spectroscopic knowledge of individual minerals accumulates, mode assignments tend to become more complex.

Rather than approximating the spectrum of an isotopically light mineral by a series of Einstein oscillators, as has been common in previous models cited above, I have used a refinement of the model proposed in papers 3 and 4, subdividing the spectrum of each mineral considered into various groups of vibrational modes characteristic of the minerals, as shown schematically in Figure 6. In general, I have used more detailed approximations to the mineral spectra for the purpose of calculating isotopic fractionation factors than I did for calculation of thermodynamic variables and phase equilibria. This greater detail is necessary in order to identify and isolate modes that might have common frequency shifts upon isotopic substitution. The heavy line in Figure 6 represents the spectrum of an isotopically light mineral. The

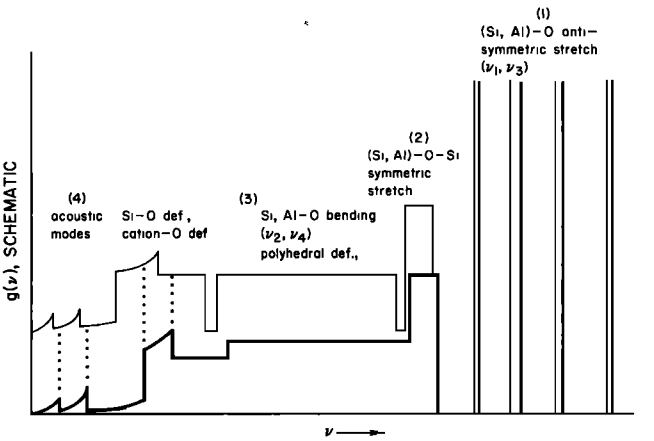

Fig. 6. Schematic vibrational spectra used for the isotopically light mineral (heavy bottom line) and the isotopically heavy mineral (light upper line).

major groups of vibrations identified for each silicate mineral are (in approximate order of decreasing frequency) (1) tetrahedral antisymmetric stretching modes, denoted as ν_1 and ν_3 in the vibrations of an isolated tetrahedron, (2) symmetric stretching modes, often termed 'bridging deformations,' (3) tetrahedral bending modes, (4) polyhedral, Si-O, and cation-oxygen 'deformations,' and (5) acoustic modes. Acoustic modes are represented as in papers 3 and 4 by one longitudinal and two shear modes which are assumed to obey a simple sine dispersion law between wave vector and frequency. Optic modes are represented in two ways: (1) where justified and possible, by Einstein oscillators, for example, for Si-O stretching modes, internal carbonate modes, and hydroxyl stretching modes, and (2) by an optic continuum or segmented continua as shown in Figure 6. The number of modes of each type and their frequency or frequency range must be specified from data in the spectroscopy literature, or, too often, from interpretation or extrapolation of these data. As will be demonstrated below, application of the model is often limited by lack of spectroscopic data, or by lack of mode assignments to existing data, and much more data and interpretation are needed.

Once these groups of modes have been defined and enumerated for the isotopically light mineral, a frequency shift for each group of modes must be determined to give a hypothetical spectrum of the isotopically heavy mineral. Such a shifted spectrum is shown schematically in the upper part of Figure 6 (light line). Note that different modes may be shifted by different amounts: for substitution of oxygen isotopes, the frequency may not shift if the modes do not involve displacement of oxygen atoms, whereas the frequency may decrease as much as 94.3% [$= (16/18)^{1/2}$] if the modes involve only motions of oxygen atoms.

Because normal mode frequencies and deformation types depend in detail on the geometry of the vibrating unit or cluster, a detailed calculation of the effect of isotopic substitution in principle requires a detailed model of force constants for lattice vibrations. However, as shown in papers 1–4, a useful approximation is that the vibrations of individual clusters of atoms can be enumerated and characterized. *Herzberg* [1945, pp. 227–238] discussed models for the vibrations of isolated molecules of the form XY_2, XYZ_3, and XY_4. These models give solutions for frequency that can be

TABLE 2. Frequency Decreases Assumed for Silicates When ^{16}O Is Replaced by ^{18}O

Mineral Class	Antisymmetric (Si, Al)-O Stretch (Rule 1)	Symmetric (Si, Al)-O-Si Stretch (Rules 2, 5)	Bending, Distortion, Other (Rules 3, 5)	Acoustic (Rule 4)
Framework	0.96	0.99 for those identified; *HT* limit for those at low frequency (see text)	*HT* limit[a]	$(M/M^*)^{1/2}$[b]
Sheet	0.96	0.99	*HT* limit	$(M/M^*)^{1/2}$
Chain	0.96	0.99	*HT* limit	$(M/M^*)^{1/2}$
Orthosilicates	$\nu_1 = 0.943$ $\nu_3 = 0.977$	not present	bending modes, 0.95 other: *HT* limit	$(M/M^*)^{1/2}$

[a] *HT* limit (high-temperature limit): see equations (20) and (21) and discussion.
[b] M is the formula weight; the asterisk denotes the isotopically heavy mineral.

used to estimate the dependence of frequency on atomic mass of various atoms in the cluster. Although complete solutions for frequency shifts of clusters of all compositions imaginable in minerals are currently beyond reach, Herzberg's calculations and considerations of end-member types of vibrations can be used to provide an estimate of the expected shifts in those cases where the vibrations are fairly well isolated in frequency, for example, for Si-O antisymmetric stretching modes and for internal modes of the carbonate ion.

For vibrational modes not well approximated by the vibrations of an isolated cluster, various considerations were used to construct the rules presented below for frequency shifts. The advantage of these rules is that they can be applied uniformly to a wide variety of minerals having different structural and compositional characteristics. The set of partition functions thus obtained is internally consistent, but values will change as more is learned about the shift factors or as spectra are treated with higher resolution or more detail. The disadvantage of these rules is that they are not based on detailed consideration of the atomic structure.

Frequency Shifts Upon Isotopic Substitution: A Simple Set of Rules for Silicates

Groups of modes treated separately are listed in Table 2. Although various groups of modes can overlap in frequency (as discussed, for example, in paper 4), such overlaps generally involve only a few modes and are largely ignored here for simplicity; one exception is Si-O symmetric stretching modes discussed below. For reasons that will become clear at the end of the section, the modes are discussed below in the order (1) antisymmetric stretching modes, (2) symmetric stretching modes, (3) bending modes, (4) acoustic modes, and (5) other deformational modes.

Rule 1 (antisymmetric (Si, Al)-O stretching modes): If ν_1 and ν_3 modes can be separately identified and enumerated, their frequencies are assumed to decrease by 0.943 and 0.977, respectively, upon substitution of ^{18}O for ^{16}O. If they cannot be separately enumerated, an average shift of 0.96 is used for the antisymmetric modes.

The (Si, Al)-O antisymmetric stretching modes are those called ν_1 and ν_3 when they can be identified in isolated molecules or orthosilicates. In relatively isolated molecules, the shift of ν_1 is very simple [*Herzberg*, 1945]:

$$\frac{\nu_1}{\nu_1^*} = \left(\frac{^{16}m}{^{18}m}\right)^{1/2} = 0.942809 \sim 0.943 \qquad (18)$$

The shift of ν_3 is more complex, depending not only on the relative masses of oxygen isotopes, but also on the relative shift of the ν_4 (bending) mode. *Herzberg*'s [1945, p. 182] valence-force model can be used to derive a set of simultaneous equations for ν_1/ν_1^*, ν_2/ν_2^*, ν_3/ν_3^*, and ν_4/ν_4^*. These equations can be solved for ν_3/ν_3^* if the ratios ν_1/ν_2 and ν_3/ν_4 of isotopically light minerals are known. These two ratios vary in minerals because they depend on cation masses and force constants (note that this fact shows the weakness in the assumption that molecular clusters can be treated as isolated clusters). Values of $\nu_1 = 819$, $\nu_2 = 340$, $\nu_3 = 956$, and $\nu_4 = 527$ cm^{-1} [from *White*, 1975, p. 328] are typical, although the spread of proposed values may be as much as 200 cm^{-1} for any one mode. With these values, the calculated ratio ν_3/ν_3^* is 0.977, and this value is used throughout this paper. For orthosilicates I assumed that the ratio of the number of ν_3 to ν_1 modes was 3:1, as it would be for an isolated tetrahedron.

For silicates in which the tetrahedra are partially to completely polymerized, separate identification of the antisymmetric vibrational modes as ν_1 and ν_3 is not possible, or perhaps, even meaningful. Therefore a general rule for calculation of the shift of ν_1 and ν_3 antisymmetric mode frequencies resulting from ^{18}O substitution cannot be given for polymerized silicates. However, a few data do exist. A shift of 0.96 was observed experimentally for these modes in thin films of vitreous silica [*Ligenza and Spitzer*, 1960]. *Kawabe* [1978] gave a detailed model for oxygen-isotope fractionation in quartz, and the weighted average of his calculated shifts of these modes is 0.9575. Therefore it is probably reasonable to assume a shift of 0.96 for the antisymmetric stretching modes of SiO_4^{-4} tetrahedra for the framework silicates. It is assumed to be the same for AlO_4^{-5} tetrahedra. No data exist to test the validity of this assumed shift for silicates of intermediate polymerization. However, the fact that the weighted averages of the ν_1 and ν_3 shifts for isolated tetrahedra and polymerized tetrahedra are so similar suggests that values near 0.96 should apply to the Si-O-Si antisymmetric stretching modes rather independently of degree of polymerization of tetrahedra.

Rule 2 (symmetric (Si, Al)-O-Si stretch): The frequency shift of symmetric (Si, Al)-O-Si stretching modes upon substitution of ^{18}O for ^{16}O is taken to be 0.990, for those modes involving mainly Si motion; some modes, by accidents of mineral symmetry, become deformational modes and must be treated differently.

In minerals containing bridging oxygens, there are some Si-O-Si stretching modes whose deformations involve primarily motion of Si; these are usually called symmetric Si-O-Si or Si-Si stretching modes in spectroscopic assignments. The method of enumerating these modes was given in paper 4; I assume that one symmetric Si-O-Si stretch exists for each Si-O-Si bond.

In the quartz spectrum, five of the six expected modes have been found between 697 and 807 cm^{-1} [*Lippincott et al.*, 1958; *Becker*, 1971]: at 807, 795, 778, and 697 (doubly degenerate) cm^{-1}. These modes should show very little frequency shift upon substitution of oxygen isotopes. Although no data are available on quartz, the same modes are present in vitreous silica, and the spectral data of *Ligenza and Spitzer* [1960] show a frequency shift of only 0.9868 upon substitution of oxygen isotopes. I have rounded this to 0.990 in my model.

The sixth Si-O-Si deformational mode in quartz becomes an O-Si-O deformation or Si-O bending mode at an anomalously low frequency, 466 cm^{-1} [*Moenke*, 1974, p. 366], because motion of Si is not permitted in the A_1 species to which this mode belongs. *Kawabe* [1978, p. 616] calculated a shift of 0.945 for this mode; I placed this mode in the continuum with other distortional modes (between 90 and 550 cm^{-1}; Table 3) and determined the shift for this group from the high-temperature product rule (discussed below). The average shift for this group is 0.949917 ~ 0.950, which gives a shift for this one mode in good agreement with that calculated by Kawabe.

In the feldspars, 16 (Si, Al)-O-(Si, Al) symmetric stretching modes would be expected. According to *Lazarev* [1972, p. 182], eight should be infrared active, and he finds these eight to be between 500 and 800 cm^{-1}; these frequencies, as

TABLE 3. Range of Modes, q, and Frequency Shift Assumed for Calculations of Oxygen Isotope Fractionation

	ν_{as} Si-O			ν_s Si-O-Si or, for Orthosilicates, Si-O Bending Modes			Lattice Distortion			
Mineral	Range	q	Shift	Range	q	Shift	Range	q	Shift	Acoustic
Quartz	1200	0.074		697–809	0.1852	0.99	90[a]–550[b]	0.4817	0.949917	
	1162	0.037	0.96							0.968246
	1117	0.074								
	1080	0.037								
Albite	1010	0.051	0.96	720–780	0.1025	0.99	500–650	0.1025	0.961462	
	1123	0.154	0.96		0.1025	0.99	and			0.970797
							63–476	0.5515	0.961462	
Anorthite	960	0.051	0.96	666–770	0.1025	0.99	460–620	0.1025	0.961367	
	1070	0.154	0.96				and			0.972429
							85–410	0.5515	0.961367	
Muscovite	3633	0.032	0.996	700–900	0.095	0.99	91–620	0.6902	0.963671	
	1000	0.159	0.960							0.971170
Clinoenstatite	1000	0.100	0.960	650–750	0.067	0.99	170–563	0.683	0.964254	
	900	0.100	0.960							0.971398
Diopside	1000	0.100	0.96	610–710	0.067	0.99	128–557	0.683	0.963853	
	900	0.100	0.96							0.973328
Pyrope	975	0.15	0.977	450–630	0.25	0.95	115–450	0.5375	0.971167	0.971503
	875	0.05	0.943							
Grossular	950	0.15	0.977	450–619	0.25	0.95	152–450	0.5375	0.971100	0.974379
	850	0.05	0.943							
Andradite	925	0.15	0.977	450–589	0.25	0.95	116–450	0.5375	0.971035	
	825	0.05	0.943							0.977192
Zircon	974	0.055	0.943	400–608	0.275	0.95	185–400	0.4217	0.962066	0.971503
	1000	0.100	0.977							
	885	0.055	0.977							
Forsterite	930	0.142	0.977	420–650	0.238	0.95	128–420	0.5363	0.973624	0.972710
	837	0.048	0.943							
Rutile	824	0.167	0.96	450–500	0.222	0.990	80–450	0.389	0.940418	0.975871
	610	0.055	0.96							

	Internal Carbonate Modes			External Modes			External Modes			
Mineral	Range	q	Shift	Range	q	Shift	Range	q	Shift	Acoustic
Calcite[c]	1460	0.133	0.9837	300–387	0.100	0.970	200–325	0.200	0.982260	0.971311
	1070	0.067	0.9427				and			
	881	0.067	0.9888				77–200			
	712	0.133	0.9476					0.200	0.943	

[a]Lower limit of optic continuum cited is that at $\mathbf{K} = \mathbf{K}_{max}$. This corresponds to the lowest IR or Raman mode at $\mathbf{K} = 0$ modified by an assumed dispersion curve across the Brillouin zone as discussed in paper 3.
[b]$\mathbf{K}_{max}$ from *Elcombe* [1967].
[c]Data for calcite partially from *Bottinga* [1968].

well as the antisymmetric (Si, Al)-O stretching frequencies, are lower than the corresponding frequencies in quartz because the substitution of Al for Si into the structure lowers its rigidity and, hence, vibrational frequencies. *Iiishi et al.* [1971] further subdivide these modes into Si-Si or Si-Al(Si) stretching between 720 and 780 cm^{-1} and O-Si(Al)-O bending between 500 and 650 cm^{-1}. The diagrams shown by Iiishi et al. for vibrational modes suggest that the symmetric (Si, Al)-O-(Si, Al) vibrations of feldspars resemble those of quartz: The ones between 720 and 780 cm^{-1} involve mainly motion of silicon, whereas those at the lower frequency involve considerable motion of oxygen and, in fact, merge into other types of deformational modes. Accordingly, I have taken half of the (Si, Al)-O-(Si, Al) symmetric stretching modes of feldspars to lie in the higher-frequency group (720–780 cm^{-1} for albite; 666–770 cm^{-1} for anorthite) with a shift of 0.99. I have taken the other half at lower frequencies (500–650 cm^{-1} for albite; 460–620 cm^{-1} for anorthite) combined with other deformational modes and have determined their frequency shift by the high-temperature product rule discussed below.

Rule 3 (Si-O bending modes in orthosilicates): If the Si-O bending modes in orthosilicates can be identified and enumerated, their frequency shift upon substitution of ^{18}O for ^{16}O is taken to be 0.95.

In orthosilicates the Si-O bending modes of isolated tetrahedra can be identified and enumerated. The isolated tetrahedron has 1.25 times as many bending modes ($\nu_2 + \nu_4$) as antisymmetric stretching modes ($\nu_1 + \nu_3$). The same relative proportions are used here. Consideration of deformation of an isolated tetrahedron indicates that $\nu_2^*/\nu_2 = 0.943$ and $\nu_4^*/\nu_4 = 0.949$ [*Herzberg*, 1945]. The weighted average shift for the modes would be 0.947. A value of 0.95 was adopted for this model. This shift is very large because the bending modes for an isolated tetrahedron involve principally the motions of oxygen (remember that the maximum possible shift is 0.943 for modes involving only motions of oxygens). If the motions of oxygen are hindered either by interactions with the cations or by polymerization of the bonds, the shifts should be less; indeed, the only data available on a framework silicate, vitreous silica [*Ligenza and Spitzer*, 1960], give a value of 0.966 for the bending modes.

Rule 4 (acoustic modes): The ratio of frequencies upon substitution of ^{18}O for ^{16}O is taken to be proportional to the square root of the ratio of the mean molecular masses.

The lowest-frequency modes, the acoustic modes, are the last group of modes for which a frequency shift can be estimated on empirical or theoretical considerations. At long wavelengths the fundamental vibrating unit is the primitive unit cell, and, by analogy with the vibrations of a monatomic chain (paper 1, equation (20)), the ratio of acoustic frequencies of isotopically heavy and light minerals is $\omega^*/\omega = (M/M^*)^{1/2}$, where M denotes the total mass of the unit cell or, in the ratio of masses, can be taken to be the formula weight. The mineral molar volume, which is required for calculation of the acoustic mode frequencies (equations (8), paper 3), is assumed to decrease linearly with the molecular-mass ratio.

Rule 5 (remaining undifferentiated modes): The frequency shift of the remaining modes upon substitution of ^{18}O for ^{16}O is determined from the high-temperature product rule that requires that the fractionation go to zero at high temperatures.

The groups discussed above account for roughly 40–50% of the modes of typical silicates. The remaining modes are of several types: lattice deformations and distortions, polyhedral deformations, tetrahedral bending modes, and, in some minerals, OH-bending or librational modes. The shift to be applied to this remaining group of modes is not arbitrary. Because fractionation is required to approach zero at high temperature, frequency shifts must obey the high-temperature product rule [*Becker*, 1971], derived from (9) and (10) by taking the high-temperature limit:

$$\prod_{i=1}^{3s} \frac{x_i}{x_i^*} = \left(\frac{m^*}{m}\right)^{3r/2} \tag{19}$$

where s is the number of atoms per unit cell, r is the number of atoms being exchanged in the isotopic reaction, m is the mass of the exchanging atom, and the asterisk denotes the heavy isotope. This rule can be rewritten as

$$\sum_{i=1}^{3s} \ln (x_i/x_i^*) = \frac{3r}{2} \ln (m^*/m) \tag{20}$$

If the spectrum is broken into parts containing $a, b, c, d, \cdots$ modes, each part having a common frequency shift (i.e., $x_i/x_i^* = \text{const } K_a, K_b, K_c, K_d, \cdots$), then this equation becomes

$$a \ln K_a + b \ln K_b + c \ln K_c + d \ln K_d + \cdots = \frac{3r}{2} \ln (m^*/m) \tag{21}$$

Thus if all weighting factors $a, b, c, d, \cdots$ are known and if all shifts but one (e.g., K_d) are known, the unknown shift can be obtained from the above equation. This approach was used by *Becker* [1971] to determine the relation between the shift assumed for the acoustic modes and that of the lowest-frequency optic modes for quartz. It is used here to determine the shift of the modes remaining after identification of all others by the procedures described above.

The spectral shifts used for the minerals are summarized in Table 3. The shift shown to six decimal places (other than the acoustic mode shift) is the shift determined by the high-temperature rule; this degree of accuracy is necessary to ensure convergence in the numerical results.

Calcite was included in this study in order to compare this model with the previous calculations of *Bottinga* [1968]. For this comparison, the shifts of all modes except 20% between 200 and 325 cm^{-1} were taken to be similar to Bottinga's shifts; the shift of the modes between 200 and 325 cm^{-1} was determined by the high-temperature product rule. As Bottinga derived shifts for these modes in a different way, this comparison provides a test of the use of the high-temperature product rule for representing average shifts. Four internal modes of the carbonate ion were identified and considered as Einstein oscillators: ν_1 at 1070 cm^{-1}, ν_3 at 1460 cm^{-1}, ν_2 at 881 cm^{-1}, and ν_4 at 712 cm^{-1}. From the *Herzberg* [1945, p. 177] model for the carbonate ion and the observed frequencies given above, one can calculate a theoretical shift for the internal mode frequencies of an

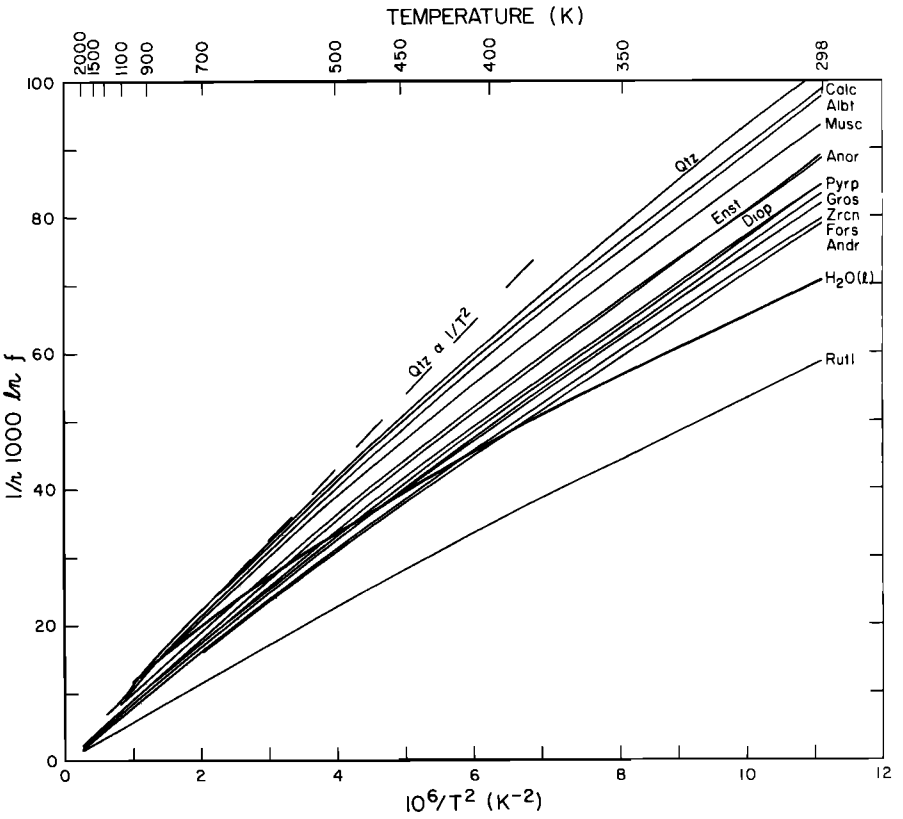

Fig. 7. Reduced partition function versus $1/T^2$ (bottom axis) or T (top axis); r is the number of exchangeable oxygens in the unit cell of the mineral. The heavy curve labeled $H_2O(l)$ is the reduced partition function of 'liquid' water from *Becker* [1971]. The dashed curve shows a T^{-2} extrapolation of the high-temperature quartz curve to emphasize the curvature of the curves at low temperature. The mineral abbreviations are as follows: Qtz (quartz), Calc (calcite), Albt (albite), Musc (muscovite), Enst (clinoenstatite), Anor (anorthite), Diop (diopside), Pyrp (pyrope), Gros (grossular), Zrcn (zircon), Fors (forsterite), Andr (andradite), and Rutl (rutile).

isolated carbonate ion upon substitution of ^{18}O: ν_1^*/ν_1 = 0.942809, ν_2^*/ν_2 = 0.988826, ν_3^*/ν_3 = 0.99063, and ν_4^*/ν_4 = 0.941093. Bottinga, using a more detailed model, obtained very similar values: ν_1^*/ν_1 = 0.942682, ν_2^*/ν_2 = 0.988797, ν_3^*/ν_3 = 0.983664, and ν_4^*/ν_4 = 0.941093. Therefore, to simplify comparison of my model with Bottinga's work, I used the latter values, because the major differences between our two models are in the remaining part of the spectrum. This remaining part of the calcite spectrum was divided into three regions. From 99 cm^{-1} (at K = 0) to 200 cm^{-1}, modes involve only motions of the oxygens about the central carbon atoms, which remain stationary [see *White*, 1974, p. 231]. I therefore assumed that the frequency shift is $(16/18)^{1/2}$ = 0.943; Bottinga found a similarly large shift for most of these modes. Near 300 cm^{-1} (300–387 cm^{-1} if longitudinal and transverse frequencies are included), three modes ν_6 and ν_8 (doubly degenerate) exist [*White*, 1974, p. 233], and all involve opposing motions of the calcium atoms and carbonate ions, in either compression or shear. I assumed that the frequencies of such modes might scale with the square root of reduced mass of the calcium atom and the carbonate ion; this assumption would give a shift of 0.982. Bottinga's average shift for these three modes was 0.970. The latter value was used. The shift of the remaining modes between 200 and 325 cm^{-1} was determined from the high-temperature product rule, equation (21) above, to be 0.982260.

Results

The results of the model are shown in several ways in Figures 7 and 8 and in Table 4. In Figure 7 the reduced partition function, $1/r$ 1000 ln f, is plotted against $1/T^2$. In Figure 8 the fractionation between quartz and the other minerals studied is plotted against $1/T^2$. In Table 4, values of the mineral-water fractionations at 298° and 1000°K are given and compared with experimental data where available. Values of the reduced partition function of water used for this calculation are those of *Becker* [1971, p. 52]: at 298.16°K, 1000 ln f is 70.81, and at 1000°K it is 11.55.

The model predicts correctly that the reduced partition function of the minerals changes systematically with structure, as first explained by *Taylor and Epstein* [1962]. For anhydrous silicates, it decreases in the order framework, chain, and orthosilicates as shown in Figure 7. This order reflects the decreasing frequency of the antisymmetric Si-O stretching modes with this structural progression. Calcite has a high reduced partition function because of the high frequencies of the internal carbonate ion; rutile has a low partition function because of the low frequencies of the Ti-O modes.

In detail, the relative order of the reduced partition functions is slightly different from those orders determined by experiment, but the differences only occur where differences in the reduced partition function are of the order of

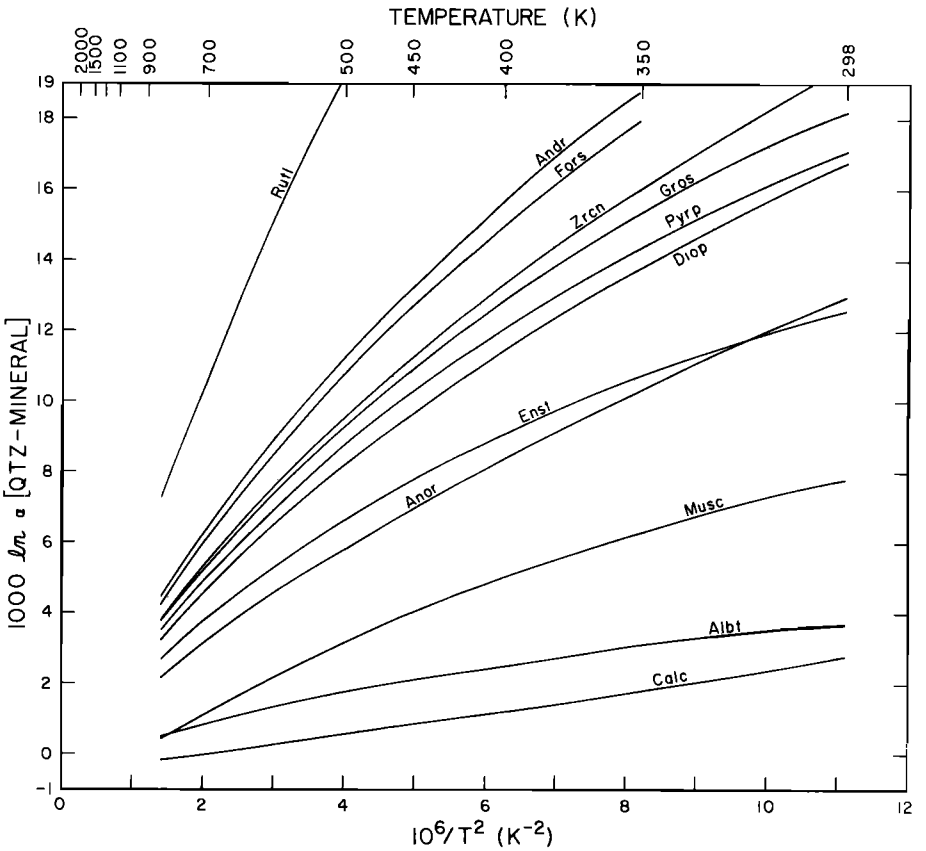

Fig. 8. Fractionation factors between quartz and the minerals indicated (abbreviations are the same as in Figure 7) versus $1/T^2$.

1‰. For example, the order predicted by the model at 298°K is quartz > calcite ≳ albite > muscovite > enstatite ≈ anorthite, whereas *Taylor* [1974, p. 846] gives quartz > albite > calcite for the first three. At 800°K, just below the α-β quartz transition, the model predicts the order quartz ~ calcite > albite ~ muscovite > anorthite > enstatite, whereas at high temperatures, Taylor gives quartz > calcite ~ albite > muscovite ~ anorthite. One difference is the value of quartz relative to calcite, and this could be accounted for by the α-β phase change, not considered in the model. This phase change would raise the reduced partition function of quartz in relation to the other minerals [*Kawabe,* 1978], bringing the predicted values into better agreement with Taylor's sequence.

It has been demonstrated that crossovers in fractionation factors in chemical compounds can occur [*Stern et al.,* 1968], but they generally do not occur in sets of minerals of comparable composition (e.g., anhydrous silicates carbonates) because of the regularity in behavior of vibrational modes with degree of polymerization of the Si-O bonds and

TABLE 4. Calculated and Experimental Mineral-Water Fractionation Factors at 298° and 1000°K

Mineral	298°K		1000°K	
	Model	Experimental[a]	Model	Experimental
Quartz	30.9	30–34	NA[b]	NA[b]
Calcite	28.1	28	−0.2	−0.2
Albite	27.2	29–30	−0.7	−0.5 → −1.0
Muscovite	23.1	17–23	−0.3	−1.0 → −1.5
Clinoenstatite	18.3		−2.2	
Anorthite	17.9	19–21	−1.9	−1.7 → −2.0
Diopside	14.1		−2.6	
Pyrope	13.8		−2.9	
Grossular	12.7		−3.0	. . .[c]
Zircon	11.4		−3.0	
Forsterite	9.1		−3.4	
Andradite	8.2		−3.5	. . .[c]
Rutile	−12.0		−5.6	−3.1

[a]Data from either *Friedman and O'Neil* [1977], *Taylor* [1974], or *Taylor and Coleman* [1968].
[b]NA is not applicable because of α-β transition.
[c]*Friedman and O'Neil* [1977] give 1000 ln α for grossular-H_2O and andradite-H_2O as −1.6 and −3.28, respectively. This model gives −3.6 and −4.2, respectively.

the monotonic dependence of the partition functions on this behavior. This model suggests that crossovers in fractionation factors of small magnitude can occur between pairs of structurally dissimilar minerals: for example, the small crossover between enstatite and anorthite around 325°K, between muscovite and albite around 800°K, and between calcite and muscovite at about 1100°K. The temperatures at which these crossovers occur cannot be accurately predicted because the curves intersect nearly tangentially. *Kyser* [1979] has reported a crossover between olivine and pyroxene at ~1200°C; there is no indication of such a crossover in the results of the model used here, and effects other than fractionation resulting from the harmonic properties of lattice vibrations need to be considered, such as anharmonicity or nonequilibrium effects.

The model also shows that at high temperatures the reduced partition function is proportional to $1/T^2$ as demonstrated by *Bottinga and Javoy* [1973]. However, below about 700°K the reduced partition function for all minerals is less than would be predicted by the $1/T^2$ trend. Accurate extrapolation of high-temperature data toward ambient conditions (273°K) must account for this curvature. For an example of the magnitude of the curvature effect, a difference of 20‰ from the calculated value at 298°K would be obtained by a strict $1/T^2$ extrapolation of the high-temperature quartz values.

As can be seen from Table 4, the quantitative agreement of the predicted values with data is good, except for anorthite at low temperature and rutile at high temperature. Quantitative uncertainties cannot be placed on a model of this type, which is subject to a large amount of data interpretation. My impression is that relative fractionation values for minerals that are structurally and chemically very similar (such as the albite-anorthite relations, the garnet relations) are reliable because the spectral trends are systematic, but that a larger uncertainty is associated with structurally dissimilar materials because of the difficulties in assigning mode frequencies and numbers to different types of minerals. On the basis of Table 4, I would suggest that at 298°K, differences in pairs of mineral-water fractionations are accurate to ±1‰ for structurally similar minerals and ±2‰ for structurally dissimilar minerals.

5. Effect of Pressure on the Thermodynamic Functions

The influence of pressure on thermodynamic properties of solids becomes important at mantle and core pressures. Prediction of phase boundaries at these pressures, reduction of shock wave Hugoniots for isothermal and adiabatic physical parameters, and prediction of many physical properties at high pressures are examples of problems that require estimation of the effect of pressure on such properties as heat capacity and free energy.

The following discussion is restricted to the harmonic approximation of the thermodynamic functions. At low pressures, anharmonic effects are small, but anharmonic behavior is expected to be more significant at high pressure because interatomic distances are reduced. With treatment of total free energy of an atomic system as a perturbation expansion of the harmonic energy, such as that presented by *Wallace* [1972, chapter 4], supplementation of the harmonic results discussed here with an additive anharmonic correction might be possible. At present, this requires more information than is generally available for many minerals.

Grüneisen Parameters

The harmonic thermodynamic properties change as a function of pressure because lattice vibrational frequencies shift as a result of compression. A frequently used theory is that of *Grüneisen* [1912, 1926], in which the vibrational frequencies ν_i are assumed to shift as volume according to

$$\gamma_i = -\partial \ln \nu_i / \partial \ln V \tag{22a}$$

or

$$\nu/\nu_0 = (V_0/V)^{\gamma_i} \tag{22b}$$

The quantity γ_i is referred to as the 'mode Grüneisen parameter' of the lattice vibration at frequency ν_i. Many other definitions of the Grüneisen parameter can be found in the literature, and one problem with application of the thermodynamic model of these papers to high-pressure problems is a proper choice of a Grüneisen parameter or parameters to be applied to the assumed lattice vibrational spectra.

If the lattice vibrational spectrum of a mineral were well approximated by a Debye spectrum, then Debye theory would allow a simple calculation of the effect of pressure on the thermodynamic properties, because a single Grüneisen parameter, γ_{ac}, would be appropriate; effects of pressure, temperature, and wave vector on γ_i would be ignored, and compressional and shear wave velocities would be averaged into a mean velocity. The change in the characteristic Debye frequency ν_D resulting from volume change would be assumed to be given by

$$\gamma_{ac} = -\frac{\partial \ln \nu_D}{\partial \ln V} = -\frac{\partial \ln \theta_D}{\partial \ln V} \tag{23}$$

The Grüneisen parameter appropriate here is an acoustic mode Grüneisen parameter obtained from spatial averages of the individual γ_i for the acoustic branches (denoted γ_S and γ_P) [e.g., *Anderson et al.*, 1968, p. 498]. With this assumption, the characteristic Debye frequency or Debye temperature changes with volume according to

$$\left(\frac{\nu_D}{\nu_D{}^0}\right) = \left(\frac{\theta_D}{\theta_D{}^0}\right) = \left(\frac{V_0}{V}\right)^{\gamma_{ac}} \tag{24}$$

A Murnaghan equation of state is commonly used to relate the volume change to the pressure change:

$$P = \frac{B_T}{n}\left[\left(\frac{V_0}{V}\right)^n - 1\right] \tag{25}$$

where $B_T = -V(\partial P/\partial V)_T$ and $n = (\partial B_T/\partial P)_T$. (This temporary use of the symbol n as a derivative in the Murnaghan equation should not cause confusion with its general use throughout these papers as the number of atoms in the chemical formula.) For example, for periclase, B_T = 1600 kbar, n = 4.5, and at 1000 kbar, V_0/V = 1.35. These values give $\theta_D/\theta_D{}^0$ = 1.56; thus if $\theta_D{}^0$ = 950°K, θ_D = 1430°K at 1000 kbar. The value of C_V* at 298°K and 1000 kbar is 0.59 of that at 1 bar. For corundum, the decrease would be to 0.85 of the 1-bar value and, for (metastable) quartz, to 0.86 of the 1-bar value.

As was discussed in papers 1–4, a Debye spectrum does

not represent the lattice vibrational spectra of most minerals with sufficient accuracy to be useful in problems of current interest. On the other hand, it is not generally possible to specify the real lattice vibrational spectrum, including the dependence of normal mode frequency on temperature, pressure, and wave vector. Analogously, although a single Grüneisen parameter is not likely to describe the volume dependence of the vibrational spectrum, it is not practical to specify a Grüneisen parameter for each of the $3s$ modes and to specify its dependence on temperature and wave vector. Therefore it is necessary to find a description of the way that lattice frequencies change with compression that is more accurate than permitted by Debye theory and the elastic Grüneisen parameter discussed above, yet is feasible within the context of limited data on the pressure dependence of vibrational spectra.

The work described in these papers has demonstrated that vibrational spectra have at least three distinct parts—acoustic modes at low frequencies, optical continuum modes at intermediate frequencies, and stretching modes at high frequencies—that represent very different deformational styles. One might reasonably expect that these different groups of modes might respond differently to compression, that is, might be characterized by different Grüneisen parameters. For example, as a crystal is initially compressed, the 'soft' (distortion) modes might change frequency quite drastically (γ_i large), whereas the 'hard' (stretching) modes might be relatively unaffected ($\gamma_i \approx 0$). In fact, as will be discussed below, this behavior has been observed in spectra of quartz, olivine, orthopyroxene, and garnet taken at high pressure. Thus I have attempted to formulate a theory that will describe the response of the three parts of the vibrational spectrum—acoustic, low-frequency optic, and high-frequency optic—to compression. The method of extension of this treatment to more types of modes is obvious.

In order to formulate the parameters of such a theory, assume, after *Grüneisen* [1926], that a set of parameters, γ_i, describes the changes of mode frequencies with volume according to (22*a*) and (22*b*) above. The calculation of these mode Grüneisen parameters and their averages has been a subject of much controversy (*Born* [1923], *Barron* [1955, 1957], *Schuele and Smith* [1964], *Anderson* [1968], *Knopoff and Shapiro* [1969], *Shaner* [1973], *Demarest* [1974], *Anderson* [1974], *Mulargia and Boschi* [1978], *Demarest* [1980], *Mulargia* [1980], and many others). In the quasi-harmonic approximation adopted here (in which normal mode frequencies depend on volume, but not explicitly on temperature), individual mode frequencies can be averaged according to

$$\bar{\gamma} = \frac{1}{C_V} \sum_{i=1}^{3s} \gamma_i C_{Vi} \tag{26}$$

Each mode has a characteristic γ_i, and, in principle, the γ_i are functions of the magnitude and direction of the wave vector **K**. Because this dependence is not known and because the model does not invite such intricacy, the dependence of γ_i on **K** is ignored. *Wallace* [1972, sections 32, 34] discussed this dependence briefly and gave calculated values of γ_i as a function of **K** for sodium and potassium; no experimental data exist to compare with calculated curves. For consistency with previous assumptions, I assume here that the mode Grüneisen parameters γ_i, as well as the lattice vibrational spectrum $g(\omega)$, are independent of temperature. (The reader is reminded of the discussion in paper 2 of the vibrational spectrum of rutile which has at least one highly temperature-dependent mode.) *Shaner* [1973] discussed the temperature dependence of γ_i for rutile; the temperature dependence of γ_i has also been discussed by a number of authors cited above.

Slater [1939] has demonstrated that

$$\bar{\gamma} = \gamma_{\text{thermal}} = \varepsilon V B_T / C_V \tag{27}$$

where ε is the thermal expansion and B_T is the isothermal bulk modulus. The proof by Slater does not require that the individual mode Grüneisen parameters γ_i all be equal, as frequently required by other authors for this equality. If adequate data on changes of elastic constants and infrared and Raman spectral lines with volume existed, the equality of $\bar{\gamma}$ with γ_{th} in (27) and (28) could be checked. Although such data do not exist for most minerals, data for quartz are sufficient to allow this equality to be checked (discussed below).

If (26) is rewritten explicitly in terms of the $3s$ degrees of freedom used to characterize primitive unit cells of minerals, it yields

$$\bar{\gamma} = \frac{1}{C_V} \{(\gamma_{1S} C_{V1S} + \gamma_{2S} C_{V2S} + \gamma_{3P} C_{V3P}) + (\gamma_4 C_{V4} + \gamma_5 C_{V5} + \cdots + \gamma_x C_{Vx}) + (\gamma_{x+1} C_{Vx+1} + \cdots + \gamma_{3s} C_{V3s})\} \tag{28a}$$

where the subscripts $1S$ and $2S$ indicate the two acoustic shear modes; $3P$ indicates the longitudinal mode; $4, 5, \cdots, x$ indicate the modes of the optic continuum; and $x+1, \cdots, 3s$ indicate the modes of the Einstein oscillator(s). In each case, the heat capacity is that of the mode at the temperature T at which $\bar{\gamma}$ is evaluated.

Equation (28*a*) can be written in terms of three components that indicate the cumulative contribution of the acoustic, optic continuum, and Einstein modes, respectively, to $\bar{\gamma}$:

$$\bar{\gamma} = \bar{\gamma}_{\text{ac}} + \bar{\gamma}_{\text{op}} + \bar{\gamma}_E \tag{28b}$$

where

$$\bar{\gamma}_{\text{ac}} = \frac{1}{C_V} (\gamma_{1S} C_{V1S} + \gamma_{2S} C_{V2S} + \gamma_{3P} C_{V3P}) \tag{28c}$$

$$\bar{\gamma}_{\text{op}} = \frac{1}{C_V} (\gamma_4 C_{V4} + \gamma_5 C_{V5} + \cdots + \gamma_x C_{Vx}) \tag{28d}$$

$$\bar{\gamma}_E = \frac{1}{C_V} (\gamma_{x+1} C_{Vx+1} + \cdots + \gamma_{3s} C_{V3s}) \tag{28e}$$

Note that $\bar{\gamma}_{\text{ac}}$, $\bar{\gamma}_{\text{op}}$, and $\bar{\gamma}_E$ are weighted averages of mode Grüneisen parameters and are not necessarily equal to any of the γ_i, and note the temperature dependence of the relative contributions $\bar{\gamma}_{\text{ac}}$, $\bar{\gamma}_{\text{op}}$, and $\bar{\gamma}_E$ implied in the C_V weighting factors.

Acoustic mode Grüneisen parameters, γ_{1S}, γ_{2S}, γ_{3P}. Several schemes have been devised for relating acoustic mode Grüneisen parameters (γ_{1S}, γ_{2S}, γ_{3P}) to elastic constants of the minerals. Although these schemes are based on considerations for simple, isotropic minerals, they are frequently applied to anisotropic minerals [*Anderson et al.*, 1968]; this practice will be followed here, because I have demonstrated in papers 1–4 that acoustic modes account for

so few of the total degrees of freedom for most minerals that slight errors due to averaging techniques for wave velocities will not appreciably influence the calculated thermodynamic properties.

The most common approximation [*Barron*, 1955, 1957] is

$$\gamma_i = \frac{1}{3} - \frac{V}{v_i}\left(\frac{\partial v_i}{\partial V}\right)_T = \frac{1}{3} + \frac{K_T}{v_i}\left(\frac{\partial v_i}{\partial P}\right)_T \qquad (29a)$$

where V is volume, v_i is an acoustic velocity (i = 1, 2 for shear modes; i = 3 for the compressional mode), and K_T is the isothermal bulk modulus. Another form of this equation was given by *Schuele and Smith* [1964] as

$$\gamma_i = -\frac{1}{6} + \frac{1}{2}\frac{K_T}{M_i}\left(\frac{\partial M_i}{\partial P}\right)_T \qquad (29b)$$

In this equation, M_i is the appropriate elastic modulus corresponding to the shear or longitudinal velocities. In (29*a*) the v_i are to be taken as directionally averaged sound speeds. However, as was discussed in paper 1, true directionally averaged velocities are rarely available. Furthermore, their pressure derivatives are also not available. Therefore, for implementation of (29*a*) the velocities are commonly replaced by Vogt-Reuss-Hill (VRH) averaged velocities. That convention is followed in this paper to calculate acoustic γ_i because the derivatives $\partial v_i/\partial P$ for directionally averaged modes are not known. Therefore, even though the two shear modes are taken with differing velocities in the model, the VRH shear velocity is used in conjunction with an averaged velocity pressure derivative to calculate γ_i in (29*a*). For the example of quartz to be considered here, V = 22.69 cm^3, $v_{VRH,S}$ = 4.05 km s^{-1}, $v_{VRH,P}$ = 6.02 km s^{-1} (paper 1), $(\partial v_s/\partial P) = -3.4 \times 10^{-3}$ km s^{-1} kbar^{-1}, and $(\partial v_P/\partial P) = 10.4 \times 10^{-3}$ km s^{-1} kbar^{-1} [*Anderson et al.*, 1968]. Equation (29*a*) gives $\gamma_{1S} = \gamma_{2S} = 0.023$ and $\gamma_{3P} = 1.18$ in agreement with *Anderson et al.* [1968].

Optic mode Grüneisen parameters, $\gamma_4 \cdots \gamma_{3S}$. If infrared and Raman spectra of minerals have been measured as a function of volume, then optic mode Grüneisen parameters can be calculated from

$$\gamma_i = -\partial \ln \nu_i / \partial \ln V \qquad (30)$$

Spectroscopic data [e.g., *Asell and Nicol*, 1968] demonstrate that the γ_i are generally different for the different modes and, indeed, may be positive, negative, or zero. The volume change in (30) must be measured directly or inferred from measured pressure changes through equation-of-state data.

Asell and Nicol [1968] have published frequency shifts for a sufficient number of Raman active lines of the α quartz spectrum to allow detailed examination of the γ_i of optic modes and testing of (27) and (28). Their stated highest pressure was 'about 40 kbar,' later corrected to 32 kbar (M. Nicol, personal communication, 1975). Given the pressure uncertainty and adopting several possible equations of state, the relative volume (V_0/V) at the highest pressure could have been 1.067–1.086. The compression is probably uncertain within this range, and therefore the calculations below are given for the two values; the average of the two values is taken as the most probable value. Inferred values of the Grüneisen parameter are very sensitive to volume changes and therefore to uncertainties in volume changes. The calculations of $\bar{\gamma}$ from the mode Grüneisen parameters γ_i are shown in Table 5. Within uncertainties introduced into the calculations by uncertainty in compression, the calculated value of $\bar{\gamma} = 0.73 \pm 0.09$ is remarkably close to $\gamma_{th}(0.703)$, as predicted by (27).

The relative contributions of acoustic and optic modes to $\bar{\gamma}$ can be obtained from evaluation of the three sets of parentheses in (28*c*)–(28*e*):

$$\bar{\gamma}_{ac} = 0.065 \qquad (31a)$$

$$\bar{\gamma}_{op} = 0.66 \qquad (31b)$$

$$\bar{\gamma}_E \sim 0 \qquad (31c)$$

(Values given are the mean of calculations for two values of V/V_0 as discussed in footnotes to Table 5.) The acoustic modes and high-frequency Si-O stretching modes do not contribute appreciably to $\bar{\gamma}$. The modes of the optic continuum are by far the most significant, and, in fact, as can be seen from Table 5, the two lowest-frequency optic modes alone account for much of $\bar{\gamma}$ and, therefore, γ_{th}. The relative contributions of the modes are determined (1) by the values of the mode γ_i, (2) by the values of the heat capacity weighting factors, and (3) by the relative numbers of modes. Because the modes having the largest γ_i are low-frequency modes, at room temperature their heat capacity weighting factors are relatively large, and they dominate $\bar{\gamma}$ and γ_{th}.

The contribution of Si-O antisymmetric stretching modes to the averaged Grüneisen parameter of quartz at 298°K is negligible for two reasons: (1) the heat capacity weighting factors are small, and (2) the mode Grüneisen parameters are also typically small. The mode Grüneisen parameters are small because the strong Si-O bond is relatively incompressible (for example, see discussions in the work by *Lazarev* [1972]) so that at relatively low pressures, compression is taken up by weaker bonds in the mineral structures. Therefore the frequencies of the lower-frequency modes associated with weaker bonds are most affected by overall compression. Similar behavior is observed in the few other silicates for which high-pressure spectral data are available.

Dietrich and Arndt [1982*a*, *b*] have measured the mid-infrared absorption spectrum of olivine, orthopyroxene, and garnet to 50-kbar pressure and have calculated microscopic Grüneisen parameters for the observed modes. These measurements show that the γ_i of the vibrations associated with the SiO_4^{-4} tetrahedron are small and contribute little to the macroscopic Grüneisen parameters γ_{th}. However, because the measurements do not include all infrared modes or Raman modes, the equality of $\bar{\gamma}$ and γ_{th} for these minerals cannot yet be tested through (28) and (27). Calculations of deformation of individual polyhedra in minerals, such as those of *Hazen and Prewitt* [1977] and *Hazen and Finger* [1979], when combined with spectroscopic observations, such as those of *Asell and Nicol* [1968], may eventually provide more accurate values of the mode Grüneisen parameters and allow more detailed treatment of the pressure dependence of the thermodynamic functions than is possible with current available data.

Grüneisen parameters used in model. The simplest assumption that might be used is that all mode Grüneisen parameters are equal and, from (27), are equal to γ_{th}; this will be referred to as model 1. This model is directly comparable to a Debye model, in that there is a single Grüneisen parameter, but the form of the lattice vibrational spectrum is changed from a Debye spectrum to the more realistic form proposed in paper 3.

TABLE 5. Values of γ_i for Quartz and Calculations to Demonstrate the Equivalence of $\bar{\gamma}$ and γ_{th}

ν_0, cm^{-1}	$\nu_{32\ kbar}$, [a] cm^{-1}	ν_0, [b] cm^{-1}	Mode Degeneracy	x_{0i} [c]	$\frac{C_V^*(x_{0i})}{3R}$ [d]	γ_i for $V_0/V = 1.067$ [e]	$\frac{\gamma_i C_{Vi}}{3R}$ [f]
			Optic Continuum				
128	147	128	2	0.62	0.036	2.13	0.077
207	262 ± 5	207	1	1.00	0.034	3.63	0.123
265	(~ 280)[g]	264	2	1.28	0.032	0.85	0.027
356	358	356	1	1.72	0.029	0.09	0.000
		365	1	1.76	0.029	(0.00)	(0.000)
394	395	397	2	1.92	0.027	0.04	0.001
401	407 ± 5	. . .[h]					
450	471 ± 5	452	2	2.18	0.025	0.70	0.018
464	495 ± 4	466	1	2.25	0.025	1.00	0.025
509	. . .	520	1	2.51	0.022	0.5[i]	0.011
697	720 ± 6	695	2	3.36	0.016	0.5	0.008
795	820	780	1	3.77	0.013	0.48	0.006
807	835	800	2	3.86	0.012	0.53	0.006
			Si-O Stretch				
		1055	1	5.10	0.006	0.01	0.000
1072	1073	1064	2	5.14	0.006	0.01	0.000
1085	1088	1082	1	5.22	0.006	0.04	0.000
1162	1155	1160	2	5.60	0.004	−0.09	−0.000
1231	1240 ± 10	. . .[h]					
1235	1250	. . .[h]					
			Acoustic, From Model				
S_1		102		0.493	0.036	0.023	0.000
S_2		122		0.589	0.036	0.023	0.000
P_3		164		0.792	0.035	1.18	0.041

[a]Optic mode frequencies at ambient pressure, ν_0, and at 32 kbar. The pressure was originally reported as 'about 40 kbar' by *Asell and Nicol* [1968], and was corrected to 32 kbar (M. Nicol, personal communication, 1975).

[b]Frequencies and mode degeneracies at ambient pressure, from *Lord and Morrow* [1957], given for comparison.

[c]Equal to $h\nu_i/kT$, $T = 298°K$.

[d]The heat capacity summations required for the weighting factors in (27) are $\Sigma_{i=4}^{3s} C_{Vi}^*/3R$ (for all optical modes) = 0.480; $\Sigma_{i=4}^{3s} C_{Vi}^*/3R$ (for acoustic modes) = 0.107; ΣC_{Vi}^* (total) = 3.50 cal mol^{*-1} $°K^{-1}$ in good agreement with the experimental value, 3.54 cal mol^{*-1} $°K^{-1}$.

[e]Calculated from $\gamma = -\partial \ln \nu/\partial \ln V = \ln \nu/\nu_0 \div \ln V_0/V$. If $V_0/V = 1.067$ (as in the table), $\ln V_0/V = 0.06485$. If $V_0/V = 1.087$, $\ln V_0/V = 0.0834$ and all optical mode γ_i shown in this column would be reduced to 77% of the listed value.

[f]For $V_0/V = 1.067$, $\bar{\gamma} = \Sigma\gamma_i C_{Vi}/\Sigma C_{Vi} = (0.439 + 0.0426)/0.588 = 0.82$. For $V_0/V = 1.087$, $\bar{\gamma} = 0.65$. Therefore the best estimated value of $\bar{\gamma}$, given uncertainties in compression, is the mean, 0.73 ± 0.09. For comparison, $\gamma_{th} = 0.703$ [*Anderson et al.*, 1968].

[g]Estimated by extrapolation of *Asell and Nicol* [1968] data at 20 kbar.

[h]Not seen, assumed spurious.

[i]Assumed.

A model that more nearly agrees with the spectroscopic data discussed above can be obtained by estimating separate Grüneisen parameters for acoustic and optic modes; this will be referred to as model 2. If elastic constants and thermal-expansion data are available, then (27) and (28) can be used to allow specification of acoustic and optic mode Grüneisen parameters.

Consider the three parts of (28), given as (28*c*), (28*d*), and (28*e*). The first part, (28*c*), contains the acoustic mode Grüneisen parameters which can be specified from (29*a*) or (29*b*). The second part, (28*d*), contains Grüneisen parameters appropriate to the optic continuum; these are generally unknown. They will be assumed uniform and denoted as γ_{op}, where

$$\bar{\gamma}_{op} = \sum_{i=4}^{x} C_{Vi}\gamma_{op} \div \sum_{i=1}^{3s} C_{Vi} = \gamma_{op} \sum_{i=4}^{x} C_{Vi} \div \sum_{i=1}^{3s} C_{Vi} \quad (32)$$

Equation (28*e*) contains the Grüneisen parameters appropriate to the high-frequency stretching modes; the summation over this set of parameters is assumed to be zero, either because the heat capacities of the modes at 298°K are nearly zero or because the mode Grüneisen parameters themselves are approximately zero. Then, if $\bar{\gamma} = \gamma_{th}$ as in (27), $\bar{\gamma}_{op}$ can be obtained from

$$\bar{\gamma}_{op} = \gamma_{th} - \gamma_i \sum_{i=1}^{3} C_{Vi} \div \sum_{i=1}^{3s} C_{Vi} \quad (33)$$

The individual γ_{op} to be applied to the optic continuum is then determined from (32). As an example, consider quartz: $\gamma_{th} = 0.703$, $\gamma_1 = \gamma_2 = 0.023$, $\gamma_3 = 1.18$, and $\bar{\gamma}_{ac} = 0.07$. Therefore $\bar{\gamma}_{op} = 0.63$. At 298°K the ratio of specific heats of quartz required in (32) is 0.77, so $\gamma_{op} = 0.63 \div 0.77 = 0.82$. In the calculations that follow, the values of γ used have been evaluated with heat capacity data (for (28)) and thermal-expansion data (for γ_{th}) taken at 298°K only. The error introduced by not considering the variation of the γ with temperature above 298°K is probably less than that introduced by the harmonic approximations used.

Calculation of Thermodynamic Properties at High Pressure

For the model calculations, pressure and volume are assumed to be related through a Murnaghan equation of state:

$$P = \frac{B_T}{n}\left[\left(\frac{V_0}{V}\right)^n - 1\right] \quad (34a)$$

$$V = V_0\left[\frac{nP}{B_T} + 1\right]^{-1/n} \quad (34b)$$

$$\Delta = (V/V_0 - 1) \quad (34c)$$

where B_T is the isothermal bulk modulus, n is the bulk modulus pressure derivative, and Δ is the dilatation. The Murnaghan equation of state is quite accurate at relatively low pressures (say, below the pressure equal to the bulk modulus) but is less accurate at high pressure and does not account for phase changes. More complicated and accurate equations of state, and better and more detailed values of the Grüneisen parameters (including perhaps temperature and volume dependences), could be used for minerals for which available data on physical parameters justify such treatment and the logic of the method presented here would not change.

All model parameters must be specified at the pressure under consideration. Density changes are implied by (34*b*). Acoustic velocities are assumed to change according to [*Kieffer*, 1976]

$$v_i = v_{0i}[1 - \Delta(\gamma_i - \tfrac{1}{3})] \quad (35)$$

and all characteristic optic mode frequencies are assumed to change according to

$$\nu_i = \nu_{0i}(V_0/V)^{\gamma_i} \quad (36)$$

The spectrum of vibrational frequencies thus implied is appropriate to the pressure P and volume V, and calculation of the thermodynamic functions follows from the equations of paper 3.

Results

Because data required for calculation of acoustic and optic parameters are limited, calculations are presented here for only nine of the 32 minerals of this study. The following were selected to represent different chemical compositions and structural types: halite, periclase, corundum, spinel, quartz, stishovite, rutile, forsterite, and pyrope. The Grüneisen parameters used in the three models discussed above and the bulk modulus pressure derivatives used for the calculations are given in Table 6. Because many of these minerals undergo phase changes at high pressures, the high-pressure calculations must be regarded as applying to metastable phases for most minerals.

To test the effect of using a single Grüneisen parameter to represent the shift of the optic continuum rather than individual mode Grüneisen parameters, a comparison of the model values of heat capacity for quartz was made with heat capacities obtained by considering the individual mode shifts measured at 32 kbar, by *Asell and Nicol* [1968]. Following the method of *Lord and Morrow* [1957], the optic modes of quartz were represented by 24 Einstein oscillators at the frequencies given in the third column of Table 5 for a pressure of 1 bar and in the second column for a pressure of 32 kbar. The acoustic modes were represented by three Debye distributions. The harmonic molar heat capacities at 300°K thus obtained were 10.53 cal mol^{-1} $°K^{-1}$ at 1 bar and 10.30 cal mol^{-1} $°K^{-1}$ at 32 kbar. With model 2 of this paper, the harmonic heat capacity at 300°K, 1 bar, is 10.59 cal mol^{-1} $°K^{-1}$, and that at 300°K, 32 kbar, is 10.25 cal mol^{-1} $°K^{-1}$. The <1% difference in values at 1 bar is caused by the very different nature of the vibrational spectra assumed. The important point is that in both models the heat capacity at 300°K changes by nearly the same amount: it is 97 to 98% of the 1-bar value at 32 kbar. Therefore, in at least this one case, representation of the frequency shift of the optic continuum by an averaged Grüneisen parameter does not substantially change the calculated pressure dependence of the heat capacities. The agreement is comparably good at higher temperatures.

Results of the calculations for other minerals are given in Table 7 (values of the heat capacity at 298°K for the two models and for a Debye model at 1 bar and 100, 500, and

TABLE 6. Grüneisen Parameters and Bulk Modulus Derivative Used for High-Pressure Calculations

	Model 1		Model 2				
	γ_{th} (From Literature)	γ_{th} (Model Parameters)	$\gamma_1 = \gamma_2$	γ_3	$\bar{\gamma}_{op}$	γ_{op}	$\frac{dK_T}{dP}$
Halite	1.55	1.50	0.14[a]	2.64[a]	1.05	2.19	6.00[b]
Periclase[c]	1.54	1.56	1.40	1.71	0.68	1.62	4.52
Corundum[c]	1.32	1.48	1.20	1.53	1.15	1.35	3.99
Spinel[c]	1.13	1.47	0.49	1.33	1.06	1.19	4.19
Quartz[c]	0.70	. . .[d]	0.02	1.18	0.63	0.82	6.40
Stishovite	1.00[e]	2.50[f]	0.59[f]	2.35[f]	0.71	0.95	5.00[e]
Rutile	1.50[g]	1.69	0.70[g]	0.70[g]	1.35	1.73	6.80[h]
Fosterite[c,i]	1.3[j]	1.25	0.88	1.65	1.24	1.41	4.90
Pyrope[c,i]	1.21	1.12	1.13	1.95	1.18	1.30	5.45

[a] *Schuele and Smith* [1964].
[b] *Birch* [1966].
[c] *Anderson* [1974].
[d] These model values are very uncertain because of behavior of thermal expansion.
[e] *Kalinin and Pan'kov* [1973].
[f] Estimated from $dK_T/dP = 5.6$ and $dK_T/dT = 6.9$ and the equations of *Anderson et al.* [1968] by J. Delaney (personal communication, 1979).
[g] *Shaner* [1973].
[h] *Anderson* [1974].
[i] Data of *Dietrich and Arndt* [1982*a*, *b*], available only after completion of this work, allow calculation of γ_i for two bands in the optic continuum of olivine and three for pyrope. These bands arise from bending motions of SiO_4^{-4} tetrahedra, and the γ_i are smaller than the value adopted here for the whole optic continuum. However, the SiO_4^{-4} bending modes constitute only a relatively small fraction of the modes in the continuum (see text section on isotopic fractionation), so these data are not inconsistent with the values of $\bar{\gamma}_{op}$ adopted here.
[j] *Chung* [1971].

TABLE 7. C_V^* and S_{har}^* (in cal mol^{*-1} °K^{-1}) at 298°K

	Halite		Periclase		Corundum		Spinel		Quartz		Stishovite		Rutile		Forsterite		Pyrope	
Pressure	C_V^*	S^*	C_V^*	S^*	C_V^*	S^*	C_V^*	S^*	C_V^*	S^*	C_V^*	S^*	C_V^*	S^*	C_V^*	S^*	C_V^*	S^*
								Model 1[a]										
1 bar	5.66	8.39	4.25	3.15	3.78	2.47	3.89	2.71	3.53	3.48	3.56	2.54	4.26	3.97	3.98	3.35	3.88	3.24
100 kbar	5.40	6.46	4.00	2.74	3.62	2.28	3.74	2.50	3.28	3.06	3.48	2.42	4.11	3.70	3.77	3.02	3.72	3.00
500 kbar	4.95	4.84	3.33	1.91	3.15	1.77	3.28	1.97	2.97	2.59	3.22	2.11	3.73	3.09	3.26	2.34	3.32	2.45
1000 kbar	4.66	4.19	2.84	1.46	2.74	1.41	2.90	1.62	2.82	2.38	2.99	1.87	3.45	2.71	2.89	1.93	3.04	2.11
								Model 2										
1 bar	5.66	8.39	4.25	3.15	3.78	2.47	3.89	2.71	3.53	3.48	3.56	2.54	4.26	3.97	3.98	3.35	3.88	3.24
100 kbar	5.27	6.42	4.00	2.74	3.62	2.27	3.73	2.49	3.31	3.05	3.48	2.42	4.09	3.69	3.81	3.02	3.76	3.00
500 kbar	4.53	4.79	3.30	1.91	3.13	1.76	3.24	1.96	3.00	2.57	3.22	2.12	3.67	3.07	3.36	2.33	3.42	2.44
1000 kbar	4.04	4.18	2.80	1.46	2.71	1.40	2.85	1.60	2.85	2.35	3.00	1.89	3.36	2.69	3.02	1.92	3.16	2.09
								Debye Theory										
1 bar	5.65		3.79		3.52		4.00		5.01		3.86		4.33		4.43		4.29	
100 kbar	5.40		3.53		3.36		3.84		4.81		3.77		4.16		4.23		4.11	
500 kbar	4.91		2.79		2.85		3.36		4.50		3.50		3.71		3.65		3.64	
1000 kbar	4.56		2.22		2.41		2.97		4.34		3.26		3.36		3.21		3.29	

For S_{har}^*, only the harmonic contribution to the entropy is given because the effect of pressure on the thermal expansion is not well known. Hence these numbers differ by a few percent from those in paper 4, Table 5.

[a]For model 1, all $\gamma = \gamma_{th}$. For model 2, γ_{1S} and $\gamma_{2S} = \gamma_S$; $\gamma_{3P} = \gamma_P$; γ_{op} for the optic continuum is described in the text. The parameter γ for Einstein oscillators = 0.

1000 kbar) and in Figure 9 (a plot of C_V^* versus T for the same pressures). Consider first the values of C_V^* and S^* shown in Table 7. The results of models 1 and 2 at 298°K are very similar to each other and differ substantially from Debye theory, except for halite, for which the actual and model spectra rather closely resemble a Debye spectrum (see paper 3). Debye theory does not predict accurate heat capacities for the remaining minerals; thus only the predicted relative decrease of heat capacity with pressure might have any significance. Comparison of the results of model 1 with the Debye theory shows the effect of differing vibrational spectra because both model 1 and Debye theory use the same Grüneisen parameter, γ_{th}, for all modes.

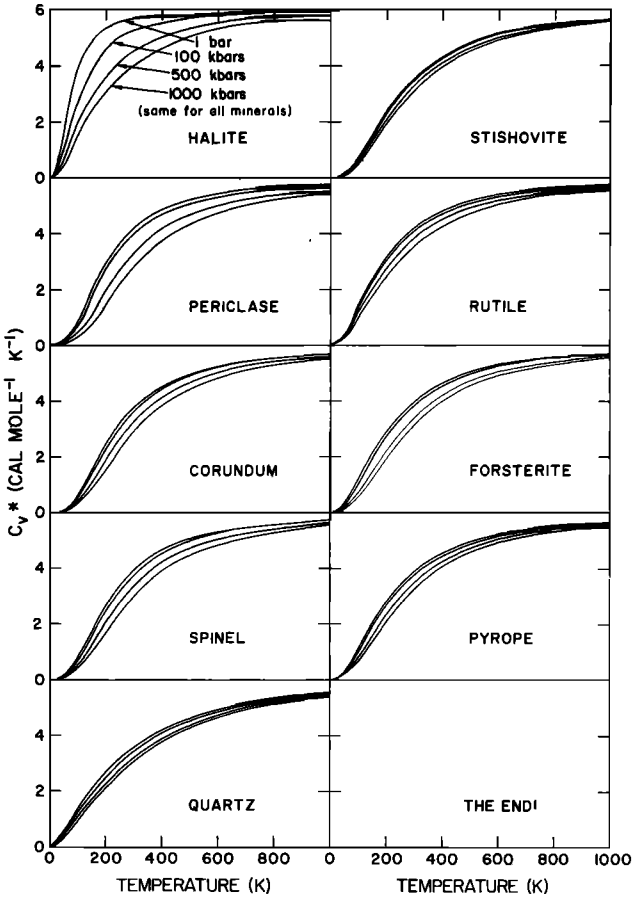

Fig. 9. Model heat capacities of various minerals (or their metastable low-pressure phases) at pressures of 1 bar and 100, 500, and 1000 kbar.

With the exception of halite, models 1 and 2 do not give significantly different results for C_V^* and S^* at 298°K, an initially surprising result because of the apparent large differences in Grüneisen parameters used in the two models. However, in a general way, this is explained by the fact that values of γ_{th} used for all modes in model 1 are rather close to the values of γ_{op} applied to the optic continuum in model 2 (Table 6). Because the optic continuum contains ≥50% of the modes, the major spectral shifts are similar in the two models, and therefore, so is the pressure dependence of C_V^* and S^*. The differences between the two models occur in two spectral regions not strongly reflected in the heat capacity or entropy at 298°K: in the low-frequency acoustic modes and in the high-frequency Einstein oscillators. At 298°K, the temperature for which the values are listed in Table 7, the acoustic modes of most minerals are nearly fully active and contribute their maximum heat capacity, regardless of the shift of their frequencies with pressure. On the other hand, at this temperature, the high-frequency Einstein oscillators contribute very little to the heat capacity, and so differences in their spectral shifts are not strongly sensed in the thermodynamic functions.

Halite is the only mineral for which the two models give substantially different pressure dependences of C_V^*. The differences arise because neither the acoustic mode nor the optic mode Grüneisen parameters are close to γ_{th}: $\gamma_1 = \gamma_2 \ll \gamma_{th}$, $\gamma_3 \gg \gamma_{th}$, and $\gamma_{op} > \gamma_{th}$. When these values of Grüneisen parameter are applied to the spectrum in model 2, the shear acoustic modes remain at lower frequencies than in model 1, and the compressional mode goes to higher frequencies (this is analogous to the way a Debye spectrum split when shear and acoustic modes were considered separately as discussed

in paper 1). The optic continuum of model 2 is shifted to substantially higher frequencies because of the high value of γ_{op}. The net effect is that model 2 predicts a stronger decrease in heat capacity with pressure than model 1. The entropy is less sensitive to these model differences because much of the entropy of halite is determined by the acoustic modes which have opposing and generally compensatory effects.

For periclase, corundum, and pyrope, the acoustic and optic mode Grüneisen parameters are all similar to γ_{th}, so models 1 and 2 are similar. For spinel, quartz, stishovite, rutile, and forsterite, the shear Grüneisen parameters are low, as in the case of NaCl, but the acoustic modes account for so few of the total degrees of freedom that the effect on γ_{op} through (33) and on the pressure dependence of the heat capacity is small.

As shown in Figure 9, the relative decrease in heat capacity at a given pressure is a function of temperature, being large on the steep part of the C_V^* curve and approaching the Dulong-Petit limit at high temperatures at all pressures. Anharmonic effects would change these high-temperature limits. Because the changes in heat capacity are large at relatively low temperatures, it is to be expected that changes in the entropy with pressure should be substantial, as is documented in Table 7.

6. Concluding Comments

The models presented in this paper for calculations of pressure effects on the thermodynamic functions, phase equilibria, and isotopic fractionation cannot be correct in detail because of the many simplifications that had to be made in the representation of physical parameters, such as the thermal expansions and the Grüneisen parameters, and in the formulation of simplified and even hypothetical spectra. The simplifications were generally necessary because of a lack of experimental data, not because of a lack of theory to incorporate the effects into the model. For example, the temperature and volume dependences of the Grüneisen parameters can easily be included in the model as presented, but available data on most minerals do not allow such a refinement; the simplified spectra can be divided and subdivided into smaller continua and more Einstein oscillators as our data base and understanding of lattice vibrational spectra increase. The work incorporated in the five papers here has spanned more than a decade, during which the data available have increased so rapidly that not all of it could be incoporated into the models. This rapid increase in data leads to hope that the current decade will be one in which continuing progress will be made in measurement of the physical properties of minerals, in understanding of their vibrational spectra, and in integration of the understanding of their physical, chemical, thermodynamic, structural, and spectroscopic properties.

Notation

The reader is referred to the notation lists at the ends of papers 1–4. Additional symbols defined below are used in this paper (equation number follows definition).

B_T isothermal bulk modulus, (25).
E_i molecular energy level, (6).
f reduced partition function ratio, (10).
K equilibrium constant, (5).
m, m^* masses of exchanging isotopes, (10); the asterisk denotes isotopically heavy substance not to be confused with the asterisk as used in C_V^* (cal mol^{*-1} $°K^{-1}$) where the asterisk denotes per atomic unit.
n bulk modulus pressure derivative, (25).
Q partition function, (5).
Q' reduced partition function, (10).
r number of atoms being exchanged in exchange reaction, (10).
α fractionation factor, (13).
Δ dilatation, (34c).
$\bar{\gamma}$ weighted average Grüneisen parameter, (26).
γ_{ac} acoustic mode Grüneisen parameter, (23).
γ_E average Grüneisen parameter for the Einstein oscillators continuum, (31c).
γ_i mode Grüneisen parameter, (22a).
$\bar{\gamma}_{op}$ average Grüneisen parameter for the optic continuum, (31b).
γ_{3P} acoustic longitudinal mode Grüneisen parameter, (28).
γ_{1S}, γ_{2S} acoustic shear mode Grüneisen parameters, (28).
γ_{th} thermal Grüneisen parameter, (27).

Acknowledgments. It has been a great pleasure to work with the editors and staff of *Reviews of Geophysics and Space Physics* during preparation of these papers, especially with associate-editor Art Boettcher and the innumerable reviewers. Helpful review comments on this paper were provided by J. Delany, R. Reeber, R. Robinson and V. Wall. The author bears full responsibility for remaining problems, and is well aware of how many were eliminated by their efforts.

References

Akimoto, S.-I., and Y. Syono, Coesite-stishovite transition, *J. Geophys. Res., 74,* 1653–1659, 1969.
Althaus, E., The triple point andalusite-sillimanite-kyanite, *Contrib. Mineral. Petrol., 16,* 29–44, 1967.
Anderson, O. L., Some remarks on the volume dependence of the Grüneisen parameter, *J. Geophys. Res., 73,* 5187–5193, 1968.
Anderson, O. L., The determination of the volume dependence of the Grüneisen parameter, *J. Geophys. Res., 79,* 1153–1155, 1974.
Anderson, O. L., E. Schreiber, R. C. Leibermann, and N. Soga, Some elastic constant data on minerals relevant to geophysics, *Rev. Geophys. Space Phys., 6,* 491–524, 1968.
Asell, J. F., and M. Nicol, Raman spectrum of α-quartz at high pressures, *J. Chem. Phys., 49,* 5395–5399, 1968.
Barron, T. H. K., On the thermal expansion of solids at low temperatures, *Philos. Mag., Ser. 7, 46,* 720–734, 1955.
Barron, T. H. K., Grüneisen parameters for the equation of state of solids, *Ann. Phys., 1,* 77–99, 1957.
Becker, R. H., Carbon and oxygen isotope ratios in iron formation and associated rocks from the Hamersley Range of Western Australia and their implications, Ph.D. thesis, Dep. of Chem., Univ. of Chicago, Chicago, Ill., 1971.
Bigeleisen, J., and M. G. Mayer, Calculation of equilibrium constants for isotopic exchange reaction, *J. Chem. Phys., 15,* 261–267, 1947.
Birch, F. C., Compressibility; elastic constants, in *Handbook of Physical Constants,* edited by S. P. Clark, *Mem. Geol. Soc. Am.,* vol. 97, 97–173, Geological Society of America, New York, 1966.
Birch, F. C., and P. LeComte, Temperature-pressure plane for albite composition, *Am. J. Sci., 258,* 209–217, 1960.
Boettcher, A. L., and P. J. Wyllie, The quartz-coesite transition measured in the presence of a silicate liquid and calibration of piston-cylinder apparatus, *Contrib. Mineral. Petrol., 17,* 224–232, 1968.
Boettcher, A. L., and P. J. Wyllie, Phase relationships in the system $NaAlSiO_4$-SiO_2-H_2O to 35 kilobars pressure, *Am. J. Sci., 267,* 875–909, 1969.
Bohlen, S. R., and A. L. Boettcher, The quartz-coesite transforma-

tion: A precise determination and the effects of other components, *J. Geophys. Res., 87,* 7073–7078, 1982.

Born, M., Atomtheorie des festen Zustandes, in *Encyklopadie der Mathematischen Wissenschaften, Physik,* vol. 3, Teubner, Leipzig, 1923.

Bottinga, Y., Calculation of fractionation factors for carbon and oxygen isotopic exchange in the system calcite–carbon dioxide–water, *J. Phys. Chem., 72,* 800–808, 1968.

Bottinga, Y., Carbon isotope fractionation between graphite, diamond and carbon dioxide, *Earth Planet. Sci. Lett., 5,* 301–307, 1969.

Bottinga, Y., and M. Javoy, Comments on oxygen isotope geothermometry, *Earth Planet. Sci. Lett., 20,* 250–265, 1973.

Boyd, F. R., and J. L. England, The quartz-coesite transition, *J. Geophys. Res., 65,* 749–756, 1960.

Boyd, F. R., P. M. Bell, J. L. England, and M. C. Gilbert, Pressure measurement in single-stage apparatus, *Year Book Carnegie Inst. Washington, 65,* 410, 1966.

Chung, D. H., Elasticity and equations of state of olivines for the Mg_2SiO_4-Fe_2SiO_4 system, *Geophys. J. R. Astron. Soc., 25,* 511–538, 1971.

Clayton, R. N., Isotopic thermometry, in *Thermodynamics of Minerals and Melts, Adv. Phys. Geochem.,* vol. 1, edited by R. C. Newton, A. Navrotsky, and B. J. Wood, pp. 85–109, Springer-Verlag, New York, 1981.

Dachille, F. D., and R. Roy, High pressure region of the silica isotopes, *Z. Kristallogr., 111,* 451, 1959.

Day, H. W., and H. J. Kumin, Thermodynamic analysis of the aluminum silicate triple point, *Am. J. Sci., 280,* 265–287, 1980.

Demarest, H., Lattice model calculation of Hugoniot curves and the Grüenisen parameter at high pressure for alkali halides, *J. Phys. Chem. Solids, 35,* 1393–1404, 1974.

Demarest, H., Comment on 'On the theoretical evaluation of the Grüneisen function in the harmonic approximation' by Francesco Mulargia, *J. Geophys. Res., 85,* 1511–1512, 1980.

Dietrich, P., and J. Arndt, Effects of pressure and temperature on the physical behavior of mantle-relevant olivine, orthopyroxene and garnet, 1, Compressibility, thermal properties and macroscopic Grüneisen parameters, *Proc. Lunar Planet. Sci. Conf.,* in press, 1982*a*.

Dietrich, P., and J. Arndt, Effects of pressure and temperature on the physical behavior of mantle-relevant olivine, orthopyroxene and garnet, 2, Infrared absorption and microscopic Grüneisen parameters, *Proc. Lunar Planet. Sci. Conf.,* in press, 1982*b*.

Elcombe, M. M., Some aspects of the lattice dynamics of quartz, *Proc. Phys. Soc. London, 91,* 947, 1967.

Elcombe, M. M., Determination of atomic eigenvector magnitudes by isotopic fractionation between sphalerite and galena using lattice dynamics, *Earth Planet. Sci. Lett., 28,* 172–180, 1974.

Elcombe, M. M., and J. R. Hulston, Calculation of sulphur isotope fractionation between sphalerite and galena using lattice dynamics, *Earth Planet. Sci. Lett., 28,* 172–180, 1975.

Epstein, S., The variations of the O^{18}/O^{16} ratio in nature and some geologic applications, in *Researches in Geochemistry,* edited by P. H. Abelson, pp. 217–240, John Wiley, New York, 1959.

Essene, E., A. L. Boettcher, and G. A. Furst, Indirect measurements of ΔG for quartz + corundum = kyanite (abstract), *Eos Trans. AGU, 53,* 554, 1972.

Friedman, I., and J. R. O'Neil, Compilation of stable isotope fractionation factors of geochemical interest, *U.S. Geol. Surv. Prof. Pap., 440-KK,* KK1–KK12, 1977.

Gaffney, E., Specific heat models of ices and clathrate hydrates, paper presented at 6th International Symposium on the Physics and Chemistry of Ice, Am. Phys. Soc., Univ. of Mo., Rolla, Mo., Aug. 2–6, 1982.

Griggs, D. R., and G. C. Kennedy, A simple apparatus for high pressures and temperatures, *Am. J. Sci., 254,* 72, 1956.

Grüneisen, E., Theorie des festen Zustande einatomiger Elemente, *Ann. Phys. Berlin, 39,* 257–306, 1912.

Grüneisen, E., Die Zustandsänderungen des festen Körpers, *Handb. Phys., 10,* 1, 1926.

Hays, J. F., and P. M. Bell, Albite-jadeite-quartz equilibrium: A hydrostatic determination, *Year Book Carnegie Inst. Washington, 72,* 706–708, 1973.

Hazen, R. M., and L. W. Finger, Bulk modulus–volume relationship for cation-anion polyhedra, *J. Geophys. Res., 84,* 6723–6728, 1979.

Hazen, R. M., and C. T. Prewitt, Effects of temperature and pressure on interatomic distances in oxygen-based minerals, *Am. Mineral., 62,* 309–315, 1977.

Herzberg, G., *Infrared and Raman Spectra of Polyatomic Molecules,* 632 pp., Van Nostrand, New York, 1945.

Hlabse, T., and O. J. Kleppa, The thermochemistry of jadeite, *Am. Mineral., 53,* 1281–1292, 1968.

Holdaway, J. M., Stability of andalusite and the aluminum silicate phase diagram, *Am. J. Sci., 271,* 97–131, 1971.

Holland, T. J. B., The reaction albite = jadeite + quartz determined experimentally in the range 600–1200°C, *Am. Mineral., 65,* 129–134, 1980.

Holm, J. L., and O. J. Kleppa, The thermodynamic properties of the aluminum silicates, *Am. Mineral., 51,* 1608–1622, 1966.

Holm, J. L., O. L. Kleppa, and E. F. Westrum, Jr., Thermodynamics of polymorphic transformations in silica, Thermal properties from 5 to 1070 K and pressure-temperature stability fields for coesite and stishovite, *Geochim. Cosmochim. Acta, 31,* 2289–2307, 1967.

Hulston, J. R., Methods of calculating isotopic fractionation in minerals, in *Stable Isotopes in the Earth Sciences,* edited by P. W. Robinson, pp. 211–219, New Zealand Department of Science and Industrial Research, Science Information Division, Wellington, N. Z., 1978.

Iiishi, K., T. Tomisaka, T. Kato, and Y. Umegaki, Isomorphous substitution and infrared and far infrared spectra of the feldspar group, *Neues Jahrb. Mineral. Abh., 115,* 98–119, 1971.

Jeanloz, R., and A. B. Thompson, Phase transitions and mantle discontinuities, *Rev. Geophys. Space Phys.,* in press, 1982.

Johannes, W., et al., An interlaboratory comparison of piston pressure calibration using the albite breakdown reaction, *Contrib. Mineral. Petrol., 32,* 24–38, 1971.

Kalinin, V. A., and V. L. Pan'kov, Equations of state of stishovite, coesite and quartz, *Izv. Akad. Nauk SSSR Fiz. Zemli, 8,* 3–16, 1973. (*Izv. Acad. Sci. USSR Phys. Solid Earth,* Engl. Transl., *8,* 495–503, 1973.)

Kawabe, I., Calculation of oxygen isotope fractionation in quartz-water system with special reference to the low temperature fractionation, *Geochim. Cosmochim. Acta, 42,* 613–621, 1978.

Kelley, K. K., et al., Thermodynamic properties of sodium-aluminum and potassium-aluminum silicates, *U.S. Bur. Mines Rep. Invest., 4955,* 1953.

Kieffer, S. W., Lattice thermal conductivity within the earth and considerations of a relationship between the pressure dependence of the thermal diffusivity and the volume dependence of the Grüneisen parameters, *J. Geophys. Res., 81,* 3025–3030, 1976.

Kieffer, S. W., Thermodynamics and lattice vibrations of minerals, 1, Mineral heat capacities and their relationships to simple lattice vibrational models, *Rev. Geophys. Space Phys., 17,* 1–19, 1979*a*.

Kieffer, S. W., Thermodynamics and lattice vibrations of minerals, 2, Vibrational characteristics of silicates, *Rev. Geophys. Space Phys., 17,* 20–34, 1979*b*.

Kieffer, S. W., Thermodynamics and lattice vibrations of minerals, 3, Lattice dynamics and an approximation for minerals with application to simple substances and framework silicates, *Rev. Geophys. Space Phys., 17,* 35–59, 1979*c*.

Kieffer, S. W., Thermodynamics and lattice vibrations of minerals, 4, Application to chain and sheet silicates and orthosilicates, *Rev. Geophys. Space Phys., 18,* 862–886, 1980.

Kieffer, S. W., P. P. Phakey, and J. L. Christie, Shock processes in porous quartzite: Transmission electron microscope observations and theory, *Contrib. Mineral. Petrol., 59,* 41–93, 1976.

Kitahara, S., and G. C. Kennedy, The quartz-coesite transition, *J. Geophys. Res., 69,* 5395–5400, 1964.

Knopoff, L., and J. N. Shapiro, Comments on the interrelationships between Grüneisen's parameter and shock and isothermal equations of state, *J. Geophys. Res., 74,* 1439–1450, 1969.

Kovach, J. J., A. L. Hiser, and C. Karr, Jr., Far-infrared spectroscopy of minerals, in *Infrared and Raman Spectroscopy of Lunar and Terrestrial Minerals,* edited by C. Karr, Jr., pp. 231–254, Academic, New York, 1975.

Kyser, T. K., The temperature dependence of oxygen isotope distributions and the origin of basalts and ultramafic nodules, *Abstr. Programs, Geol. Soc. Am., 11,* 462, 1979.

Lambert, S., Stable isotope studies of some active hydrothermal systems, Ph.D. thesis, Geol. Sci. Div., Calif. Inst. of Technol., Pasadena, Calif., 1975.

Lazarev, A. N., *Vibrational Spectra and Structure of Silicates*, translated from Russian, 302 pp., Consultants Bureau, New York, 1972.

Ligenza, J. R., and W. G. Spitzer, The mechanisms for silicon oxidation in steam and oxygen, *J. Phys. Chem. Solids, 14*, 131–136, 1960.

Lippincott, E. R., A. V. Valkenburg, C. E. Weir, and E. N. Bunting, Infrared studies of polymorphs of silica and germana, *J. Res. Natl. Bur. Stand., 61*, 61–70, 1958.

Lord, R. C., and J. C. Morrow, Calculation of the heat capacity of α-quartz and vitreous silica from spectroscopic data, *J. Chem. Phys., 26*, 230–232, 1957.

MacDonald, G. J. F., Quartz-coesite stability relations at high temperatures and pressures, *Am. J. Sci., 254*, 713, 1956.

Moenke, H. H. W., Silica, the three-dimensional silicates, borosilicates, and beryllium silicates, in *The Infrared Spectra of Minerals., Mineral. Soc. Monogr.*, vol. 4, edited by V. C. Farmer, pp. 365–382, Mineralogical Society, London, 1974.

Mueller, R. F., and S. K. Saxena, *Chemical Petrology*, 394 pp., Springer-Verlag, New York, 1977.

Mulargia, F., Reply, *J. Geophys. Res., 85*, 1513–1514, 1980.

Mulargia, F., and E. Boschi, The generalization of the Mie-Grüneisen equation of state, *Geophys. J. R. Astron. Soc., 55*, 263–267. 1978.

Navrotsky, A., Lower mantle phase transitions may generally have negative pressure-temperature slopes, *Geophys. Res. Lett., 7*, 709–711, 1980.

Newton, R. C., and J. V. Smith, Investigations concerning the breakdown of albite at depth in the earth, *J. Geol., 75*, 268–286, 1967.

Openshaw, R., The low temperature heat capacities of analbite, low albite, microcline, and sanidine, Ph.D. thesis, 312 pp., Princeton Univ., Princeton, N. J., 1974.

Ostrovsky, I. A., On some sources of errors in phase-equilibria investigations at ultra-high pressure; phase diagram of silica, *Geol. J., 5*, 321–328, 1967.

Richardson, S. W., M. C. Gilbert, and P. M. Bell, Experimental determination of kyanite-andalusite and andalusite-sillimanite equilibria; the aluminum silicate triple point, *Am. J. Sci., 267*, 259–272, 1969.

Robie, R. A., and D. R. Waldbaum, Thermodynamic properties of minerals and related substances at 298.15°K (25.0 C) and one atmosphere (1.013 bars) pressure and at higher temperatures, *U.S. Geol. Surv. Bull., 1259*, 256 pp., 1968.

Robie, R. A., B. S. Hemingway, and J. R. Fisher, Thermodynamic properties of minerals and related substances at 298.15 K and 1 bar (10^5 pascals) pressure and at higher temperatures, *U.S. Geol. Surv. Bull., 1452*, 456 pp., 1978.

Sakai, H., and H. Honma, Oxygen isotope chemistry in rock-forming processes (in Japanese), *Geol. Soc. Jpn., 5*, 9–26, 1969.

Schuele, D. E., and C. S. Smith, Low temperature thermal expansion of RbI, *J. Phys. Chem. Solids, 25*, 801–814, 1964.

Shaner, J. W., Grüneisen γ of rutile (TiO_2), *Phys. Rev. B., 7*, 5008–5010, 1973.

Slater, J. C., *Introduction to Chemical Physics*, 521 pp., McGraw-Hill, New York, 1939.

Stern, M., W. Spindel, and E. U. Monse, Temperature dependences of isotope effects, *J. Chem. Phys., 48*, 2908–2919, 1968.

Stishov, S. M., Equilibrium between coesite and the rutile-like modification of silica, *Dokl. Akad. Nauk SSSR, 148*, 153–155, 1964.

Takahashi, T., Factors influencing pressure in multi-anvil devices, in *High-Pressure Measurement*, edited by A. A. Giardini and E. C. Lloyd, p. 240, Butterworth, Woburn, Mass., 1963.

Taylor, H. P., The application of oxygen and hydrogen isotope studies to problems of hyrothermal alteration and ore deposition, *Econ. Geol., 69*, 843–883, 1974.

Taylor, H. P., and R. G. Coleman, O^{18}/O^{16} ratios of coexisting minerals in glaucophane-bearing metamorphic rocks, *Geol. Soc. Am. Bull., 79*, 1727–1756, 1968.

Taylor, H. P. and S. Epstein, Relation between O^{18}/O^{16} ratio in coexisting minerals of igneous and metamorphic rocks, 2, Applications to petrologic problems, *Geol. Soc. Am. Bull., 73*, 675, 1962.

Todd, S. S., Heat capacities at low temperatures and entropies at 298.16 K of andalusite, kyanite and sillimanite, *J. Am. Chem. Soc., 72*, 4742–4743, 1950.

Urey, H. C., The thermodynamic properties of isotopic substances, *J. Chem. Soc., 1*, 562, 1947.

Wallace, D. C., *Thermodynamics of Crystals*, p. 484, John Wiley, New York, 1972.

Weaver, J. S., D. W. Chipman, and T. Takahashi, Comparison between thermochemical and phase stability data for the quartz-coesite-stishovite transformations, *Am. Mineral., 64*, 604–614, 1979.

White, W. B., The carbonate minerals, in *The Infrared Spectra of Minerals, Mineral. Soc. Monogr.*, vol. 4, edited by V. C. Farmer, p. 227, Mineralogical Society, London, 1974.

White, W. B., Structural interpretation of lunar and terrestrial minerals by Raman spectroscopy, in *Infrared and Raman Spectroscopy of Lunar and Terrestrial Minerals*, edited by C. Karr, Jr., pp. 325–358, Academic, New York, 1975.

Yagi, T., and S. Akimoto, Direct determination of coesite-stishovite transition by *in situ* x-ray measurements, *Tectonophysics, 35*, 259–270, 1976.

Zen, E., Gibbs free energy, enthalpy, and entropy of ten rock-forming minerals: Calculations, discrepancies, implications, *Am. Mineral., 57*, 524–553, 1972.

(Received January 2, 1980·
revised July 20, 1982;
accepted July 27, 1982.)